Biochemistry

Article

Cite This: *Biochemistry* XXXX, XXX, XXX−XXX

pubs.acs.org/biochemistry

Excitation-Wavelength-Dependent Photocycle Initiation Dynamics Resolve Heterogeneity in the Photoactive Yellow Protein from *Halorhodospira halophila*

L. Tyler Mix,[†] Elizabeth C. Carroll,[†,@] Dmitry Morozov,[#] Jie Pan,[†,▽] Wendy Ryan Gordon,[∥,●] Andrew Philip,[⊥,○] Jack Fuzell,[†] Masato Kumauchi,[§,■] Ivo van Stokkum,[‡] Gerrit Groenhof,[#] Wouter D. Hoff,[*,§] and Delmar S. Larsen[*,†]

[†]Department of Chemistry, University of California, Davis, One Shields Avenue, Davis, California 95616, United States

[‡]Faculty of Sciences, Vrije Universiteit Amsterdam, De Boelelaan 1081, 1081 HV Amsterdam, The Netherlands

[§]Department of Microbiology and Molecular Genetics, Oklahoma State University, Stillwater, Oklahoma 74078, United States

[∥]Department of Chemistry and [⊥]Department of Biochemistry and Molecular Biology, University of Chicago, Chicago, Illinois 60637, United States

[#]Department of Chemistry and NanoScience Center, University of Jyväskylä, P.O. Box 35, 40014 Jyväskylä, Finland

Supporting Information

ABSTRACT: Photoactive yellow proteins (PYPs) make up a diverse class of blue-light-absorbing bacterial photoreceptors. Electronic excitation of the *p*-coumaric acid chromophore covalently bound within PYP results in triphasic quenching kinetics; however, the molecular basis of this behavior remains unresolved. Here we explore this question by examining the excitation-wavelength dependence of the photodynamics of the PYP from *Halorhodospira halophila* via a combined experimental and computational approach. The fluorescence quantum yield, steady-state fluorescence emission maximum, and cryotrapping spectra are demonstrated to depend on excitation wavelength. We also compare the femtosecond photodynamics in PYP at two excitation wavelengths (435 and 475 nm) with a dual-excitation-wavelength-interleaved pump−probe technique. Multicompartment global analysis of these data demonstrates that the excited-state photochemistry of PYP depends subtly, but convincingly, on excitation wavelength with similar kinetics with distinctly different spectral features, including a shifted ground-state beach and altered stimulated emission oscillator strengths and peak positions. Three models involving multiple excited states, vibrationally enhanced barrier crossing, and inhomogeneity are proposed to interpret the observed excitation-wavelength dependence of the data. Conformational heterogeneity was identified as the most probable model, which was supported with molecular mechanics simulations that identified two levels of inhomogeneity involving the orientation of the R52 residue and different hydrogen bonding networks with the *p*-coumaric acid chromophore. Quantum calculations were used to confirm that these inhomogeneities track to altered spectral properties consistent with the experimental results.

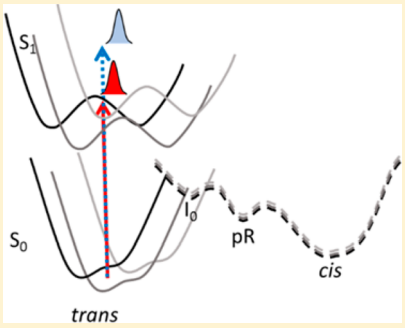

The photoactive yellow protein (PYP) family of photoreceptors consists of small single-domain proteins that are sensitive to blue-light excitation. While more than 140 members of this family have been identified in known genomes, only a few have been expressed and characterized.[1,2] The most studied representative of this family is the PYP from *Halorhodospira halophila* (Hhal PYP). Hhal PYP is a 125-residue water-soluble Per-Arnt-Sim (PAS) domain containing a thiol ester-linked *p*-coumaric acid chromophore[3] (4-hydroxycinnamic acid, or *p*CA) that gives PYP its characteristic yellow color (Figure 1). PYP naturally controls phototaxis in the purple bacterium *H. halophila*[4] and the production of biofilms in the bacterium *Idiomarina loihiensis*.[5]

Recently, PAS-containing photoreceptors such as BLUF domains (sensors of blue light using FAD), LOV (light-oxygen-voltage-sensing) domains, and PYPs[6,7] have become key targets for engineering novel optogenetic materials because they bind a variety of chromophores and enable sensory activities.[8,9] Optogenetic materials provided researchers optical control over biological processes via the engineering of foreign photoreceptors to activate or deactivate cellular functions. Examples of optogenetics include photocontrol of ionic currents, messenger molecules, and gene expression.[8,9] Photoreceptors like PYP can be linked *in vivo* to enzyme domains to create novel light-activated switches for regulating processes in biological systems.[7]

The *in vitro* photoactivity of Hhal PYP has been studied extensively since its discovery in 1987 by Meyer et al.[10] The

Received: November 2, 2017
Revised: February 15, 2018
Published: February 21, 2018

DOI: 10.1021/acs.biochem.7b01114
Biochemistry XXXX, XXX, XXX−XXX

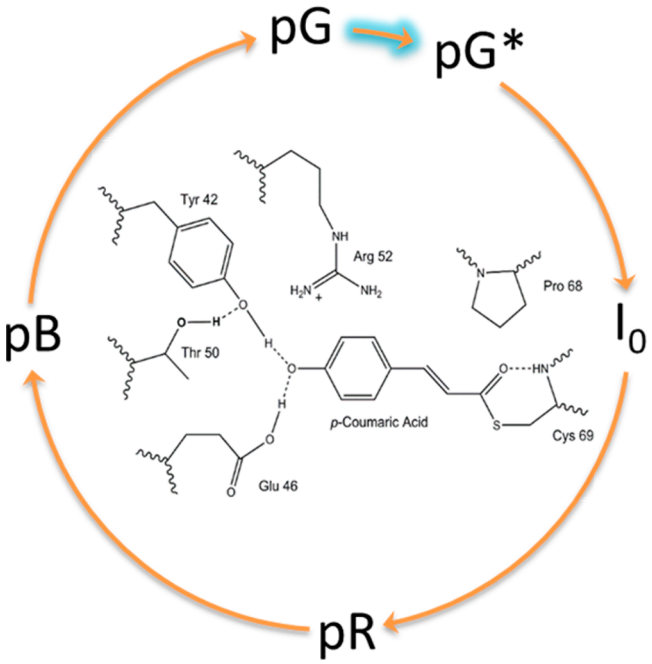

Figure 1. Simple PYP photocycle model with the protein pocket of Hhal PYP surrounding the *p*-coumaric acid chromophore.

photochemistry of PYP involves an excited-state *trans*–*cis* photoisomerization of *p*CA around the double bond that rapidly quenches fluorescence within several picoseconds and triggers a reversible photocycle (Figure 1).[11,12] Photoisomerization of *p*CA results in a temporary intermediate with a red-shifted absorption spectrum, named I_0, after tens of picoseconds.[13] The spectrum of I_0 then blue-shifts and narrows with the formation a second intermediate, called pR, within a few nanoseconds.[14] After 250 μs, the pR state is protonated to form the pB state that initiates a large scale unfolding of the protein backbone.[15,16] The protonated signaling state with altered protein geometry thermally relaxes to the starting pG state within a second[17] and is ready to begin the cycle again.

Three decades of studies of the blue-light photoactivity of PYP have resulted in a wealth of information about PYP photochemistry with more than 40 different published transient studies of wild-type (WT) Hhal PYP (Table S1).[13,18−60] These studies have used a broad range of excitation wavelengths (Figure 2) that span the entire pG absorbance spectra (black curve), with 400 nm as the most common excitation wavelength, due to its ease of generation from modern Ti:sapphire lasers. The multitude of studies at differing excitation wavelengths present a confusing picture of PYP dynamics with no agreement about the appropriate model.

From cryogenic trapping measurements, Imamoto et al. proposed a branched model that entails two pathways that separate early in the photocycle before recombining to evolve sequentially.[20] A similar heterogeneous branching model was proposed for ultrafast room-temperature dynamics from PP experiments[28] and by Mix et al.[59] from cryokinetics measurements. The observed ultrafast primary (100 fs to 10 ns) photodynamics are often multiexponential, although researchers disagree about the time scales, the amplitudes, and even the number of exponentials. For example, a mid-IR pump−probe (PP) study by Groot and co-workers identified two excited-state lifetimes for Hhal PYP photodynamics, 2 and 9 ps,[32] while visible PP measurements identified three excited-state lifetimes,

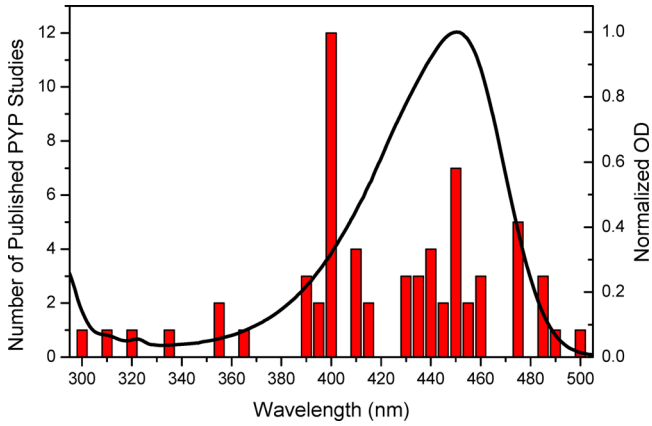

Figure 2. Hhal PYP WT pG absorbance spectrum (black) overlaid with the histogram of the number of photodynamics studies performed with a given excitation wavelength, which includes ultrafast transient absorbance, ultrafast fluorescence, low-temperature, and crystallographic techniques (Table S1).[13,18−60]

500 fs, 2 ps, and 40 ps,[24,35,59] despite both techniques resolving the same excited-state quenching dynamics. Some groups argued for a homogeneous−unidirectional−branching model from time-resolved crystallography measurements,[46,52,61] although an alternative transient crystallography study by Anfinrud and co-workers proposed a homogeneous−bidirectional−sequential model for pR production.[51] A homogeneous−unidirectional−sequential model was proposed for room-temperature evolution by Cusanovich and co-workers.[24,62] Even within sequential models, disagreements exist: a second intermediate photoproduct state, $I_0^{\ddagger}$, has been proposed between the I_0 and pR photocycle states,[13] which has not been confirmed in other PP studies. No model has been firmly established, which may be due in part to the wide range of excitation wavelengths among the experiments (Figure 2).

Despite the fact that several studies addressed the wavelength dependence of Hhal PYP photochemistry, no consensus about the interpretation of this dependence or on its biological significance, if any, has been reached. Imamoto argued because of low-temperature absorption and fluorescence signals that the yield of photochemical intermediates of PYP is dependent on the excitation wavelength.[20] It is unclear how the dynamics of cryogenically frozen Hhal PYP extend to the primary dynamics of PYP at physiological temperatures. Devanathan et al. proposed a different pathway for formation of I_0 initiated by 395 nm versus 460 nm excitation pulses but did not extend their study into the nanosecond regime required to characterize pR formation dynamics.[24] An ultrafast anisotropy experiment by Gensch et al. first revealed that photoisomerization occurs in the I_0 state with 400 and 485 nm excitation beams but did not observe pR formation dynamics.[30] Both studies clearly demonstrated that excitation wavelengths on the low- and high-energy sides of PYP's absorption band initiate different photodynamics (Figure 2, black curve).[24,30] Unfortunately, the data reported by both groups were compromised by solvated electrons created from two-photon absorption of high-energy ultrafast pulses prompting *p*CA ionization.[35] This process is an artifact of the high-intensity ultrafast excitation conditions and presumably has no significant influence on the photoresponse of PYP under ambient-light conditions but does complicate the resulting analysis with excitation wavelengths of <430 nm. Carroll et al.[48] demonstrated that PYP responds to UV light

DOI: 10.1021/acs.biochem.7b01114
Biochemistry XXXX, XXX, XXX−XXX

due to Förster resonance energy transfer (FRET) interactions with nearby Trp119 but did not investigate the wavelength dependence beyond characterizing the new initiation pathway.

Because of the limitations in published work on Hhal PYP wavelength dependence, the field would benefit from a more sensitive experimental approach for reliably quantifying excitation-wavelength dependences of PYP photochemistry that could be applied *in vivo*. Here we report a comprehensive excitation-wavelength dependence study of WT Hhal PYP using primary excited-state femtosecond dynamics, steady-state fluorescence, cryotrapped spectra, and quamtum mechanics/molecular mechanics (QM/MM) simulations to reveal and quantify excitation-wavelength dependence in the photocycle. We use an experimental method based on a dual-excitation-wavelength-interleaved pump−probe (DEWI-PP) approach[63−65] whereby two alternating broadband pump−probe signals are collected nearly simultaneously (within 4 ms) while all other experimental conditions are essentially unchanged. The DEWI-PP approach has been successfully used to resolve wavelength-dependent dynamics of cyanobacteriochromes NpR6012g4,[65] RcaE,[64] and *β*-carotene.[63] DEWI-PP removes errors caused by long-term fluctuations of excitation power, sample degradation, and different experimental conditions and constitutes a powerful approach for identifying weak but significant and potentially informative excitation-wavelength dependence of transient absorption signals.[66] Three distinct explanations for the observed wavelength dependency are considered: multiple electronic excited states, vibrationally enhanced dynamics, or heterogeneous ground and excited states.

EXPERIMENTAL METHODS

Sample Preparation. The N-terminal histidine-tagged WT apoPYP from *H. halophila* was overexpressed in *Escherichia coli* (BL21 DE3) and extracted with 8 M urea as described previously.[67,68] The apoPYP was diluted 2-fold using a 10 mM Tris-HCl buffer at pH 7.5 and reconstituted by the addition of an excess of *p*-coumaric acid anhydride (Sigma-Aldrich). After removal of the urea by dialysis against 10 mM Tris-HCl buffer at pH 7.5, the protein was purified by chromatography on a Ni-NTA resin (using 200 mM imidazole as the eluent) and DEAE-sepharose CL6B (using 100 mM NaCl for elution) until a purity index (defined as the ratio of the absorption at 446 nm to that at 278 nm) of <0.45 was achieved.

Fluorescence Spectroscopy. Fluorescence excitation and emission spectra were recorded in a SPEX Fluoromax-3 fluorimeter (Jobin-Yvon) using a cuvette with a 100 μL nominal volume (Starna #16.100F-Q-10/Z15; ∼130 μL is needed to avoid scattering from the meniscus). Because the shape of the fluorescence emission spectra of Hhal PYP is independent of excitation wavelength (Figure 3A, blue and red curves), the amplitude of the emission peak was used to estimate the wavelength dependence of the fluorescence quantum yield. This is equivalent to dividing the excitation spectrum of PYP by its absorbance spectrum. We used two approaches to confirm that inner filter effects did not perturb the observed excitation-wavelength dependence of the fluorescence quantum yield. (1) The sample concentration was adjusted to obtain an absorbance of <0.1 at the excitation wavelength, and (2) the fluorescence emission spectra were measured for samples with different PYP concentrations to ensure a linear relationship between emission intensity and sample absorbance.

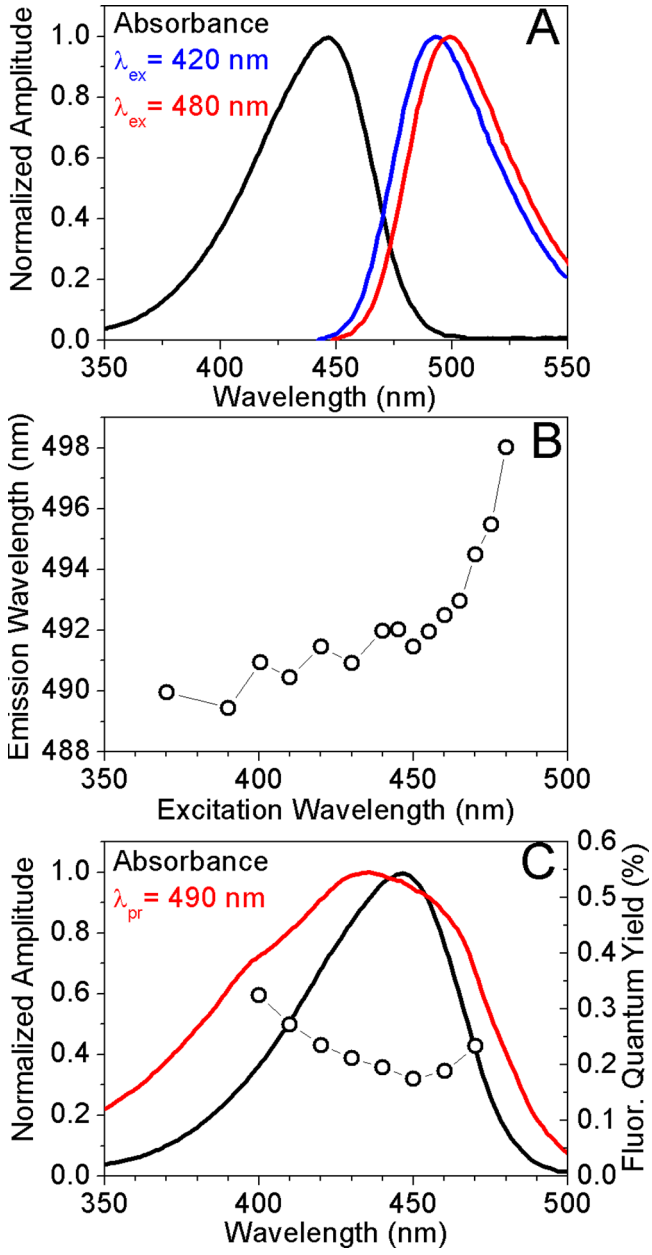

Figure 3. Wavelength dependence of the fluorescence quantum yield for wild-type PYP. (A) Absorbance spectrum of PYP (black) and emission spectra resulting from excitation of PYP at 420 nm (blue) and 480 nm (red). (B) Emission peak wavelength as a function of excitation wavelength. (C) Comparison of the absorbance (black) and fluorescence excitation spectra (red) of Hhal PYP. The quantum yield for fluorescence as a function of excitation wavelength is depicted (○, scaled according to the right *y*-axis). These data were obtained by measuring emission spectra at several different wavelengths and normalizing for the amount of absorbed light. The dotted line shows the values obtained by dividing the excitation and absorbance spectra.

Cryotrapping Spectroscopy. The low-temperature cryotrapping measurements were performed using an Oxford Instruments Optistat DN liquid nitrogen cryostat placed in the beam path of a Shimadzu UV−vis spectrometer. The PYP sample was dissolved in a solution of 66% glycerol and 33% water in a custom designed cell. The procedure for cryokinetic experiments has been described in detail elsewhere[59] and is very similar to cryotrapping. The sample is cooled to the appropriate temperature, and a reference spectrum is collected.

DOI: 10.1021/acs.biochem.7b01114
Biochemistry XXXX, XXX, XXX−XXX

Then the sample is illuminated for ~30 min with the selected pump wavelength to initiate the photocycle, and absorption spectra are collected again. The difference between the reference spectra and the illuminated spectrum at the same temperature is calculated to eliminate the influence of thermal equilibration and create spectra that resemble ultrafast transient absorption spectra for ease of interpretation.

Ultrafast DEWI-PP Absorption. The dispersed transient absorption setup was constructed from an amplified Ti:sapphire laser system (Spectra Physics Spitfire Pro and Tsunami) operating at 1 kHz, which produced 2.25 mJ pulses of 800 nm fundamental output with a 40 fs (full width at half-maximum) duration.[59,65,69,70] The 800 nm fundamental pulse train was split into multiple paths with one path generating the dispersed white-light probe supercontinuum (350−650 nm) by focusing the laser pulses into a slowly translating CaF_2 crystal. Two other paths were used to generate the 435 and 475 nm tunable visible pulses (~250 nJ) from a home-built noncollinear optical parametric amplifier (NOPA) that are impinged and overlapped, both spectrally and temporally, on the sample. The 435 and 475 nm pulses were selected to avoid contamination with solvated electrons.[35] The 435 and 475 nm pump beams were optically chopped at 500 and 250 Hz, respectively, to generate a pulse sequence in which the reference spectrum and excited spectra were collected sequentially. The illuminated spectra share the same reference spectra for the calculation of transient spectra. Both pump pulses were linearly polarized at 54.7° (magic angle) with respect to the probe pulses. The spot size diameters (~300 μm pump pulse and 50 μm probe pulses) were estimated using a micrometer stage and razor blade. The appreciably greater diameter of the pump pulse minimizes artificial contributions to the signals from a varying spatial overlap between pump and probe beams. The PYP sample was circulated through a custom 1 mm path length flow cell with 0.2 mm thick quartz windows. The overall instrument response was 125 fs as measured by the signal rise time.

Computational Analysis. The initial structure of the Hhal PYP protein was taken from Protein Data Bank (PDB) entry 2ZOH.[71] After the addition of the missing hydrogens, the protein molecule was solvated in a 6 nm × 6 nm × 6 nm periodic cube of water with six Na^+ ions to neutralize the system. The total system contained 25174 atoms. The protein geometry was minimized for 10000 steps followed by a molecular dynamics equlibration for 20 ns with 2 fs time steps using an *NPT* ensemble at a pressure of 1 bar[72] with a 1 ps time constant for pressure coupling and a compressibility of 4.5×10^{-5} bar^{-1} and a temperature of 300 K,[73] with a 0.1 ps time constant for temperature coupling. The LINCS algorithm was used to constrain bond lengths,[74] allowing a time step of 2 fs in the classical simulations. SETTLE was applied to constrain the internal degrees of freedom of the water molecule.[75] A 1.0 nm cutoff was used for nonbonded van der Waals interactions, which were modeled by Lennard-Jones potentials. Coulomb interactions were computed with the smooth particle mesh Ewald method,[76] using a 1.0 nm real space cutoff and a grid spacing of 0.12 nm. The relative tolerance at the real space cutoff was set to 10^{-5}. After equilibration, a full dynamics run for 100 ns with a 2 fs time step was performed using the same *NPT* ensemble. All structure preparations and molecular dynamics simulations were performed with the GROMACS software package[77] and parameters from the Amber03 force field with the TIP3P model of water.[78]

From the production run, snapshots with different conformations of the R52 residue and T50 hydrogen bonding network around the *p*CA chromophore were extracted. A cluster, consisting of the protein molecule with a 5 Å layer of water around it, was cut from those snapshots and run through a full scale QM/MM optimization. The quantum mechanical region consisted of the *p*CA chromophore molecule, the C69 residue, and side chains of amino acids Y42, E46, and T50 (68 atoms in total). To estimate the effect of the R52 conformation on the excitation energies, the side chain of that amino acid was later included in the QM region. The QM/MM interface between the GROMACS package and the GAMESS(US) quantum chemistry package[79] was employed to perform this optimization using density functional theory with the PBE0/cc-pVDZ[80] basis set and Amber03 force field. After optimization, the vertical excitation energies (VEEs) were computed using second-order extended multiconfigurational quasi-degenerated perturbation theory (XMCQDPT2)[81] using a five-state averaged complete active space self-consistent field (CASSCF)[82] wave function as a reference. The active space in these CASSCF calculations included the 11 π-orbitals of the chromophore and 12 electrons [i.e., XMCQDPT2/SA(5)-CASSCF(12,11)/cc-pVDZ]. The VEEs and oscillator strengths were computed with Firefly version 8.2.[83]

RESULTS

Static Fluorescence. Hhal PYP is weakly fluorescent with fluorescence quantum yields (Φ_f) that are <0.5% but exhibit a clear excitation-wavelength dependence in the emission and excitation spectra (Figure 3). The emission maximum of Hhal PYP changes slightly as a function of excitation wavelength, with shorter excitation wavelengths producing shorter emission wavelengths (Figure 3A,B). Excitation on the far blue edge of the absorbance spectrum at 370 nm generates emission at 490 nm, while 480 nm excitation produces emission at 498 nm. The largest changes in the peak position of the emission spectra occur upon excitation above 460 nm, on the red flank of the absorbance band. However, the shape, including bandwidth and shoulder, of the fluorescence emission spectra is largely independent of excitation wavelength (Figure 3A). The characteristics of the excitation spectrum measured at 490 nm (Figure 3C) provide further evidence of wavelength-dependent fluorescence. The excitation spectrum (red curve) is substantially broader than the absorbance spectrum (black curve), with clearly enhanced amplitudes on the flanking edges.

The wavelength dependence of the fluorescence quantum yield (Φ_f) was determined in two ways. First, the excitation-wavelength-dependent amplitude of the emission peak was normalized to the sample absorbance. Second, the measured excitation spectrum of Hhal PYP was divided by its absorbance spectrum. Both approaches yield nearly identical results [Figure 3C (○)]. The value of Φ_f is smallest near 450 nm and increases upon excitation with light on both the blue flank and the red flank of the Hhal PYP absorbance band. Hence, both higher-energy excitation, 400 nm, and lower-energy excitation, 480 nm, result in up to twice as much emission as excitation at the pG absorbance peak, 440 nm. Because the observed dependence of fluorescence quantum yield on excitation wavelength resembles the absorbance spectrum, we performed additional measurements at multiple reduced sample concentrations, demonstrating that inner filter effects did not contribute to the fluorescence yields in Figure 3C (data not shown).

DOI: 10.1021/acs.biochem.7b01114
Biochemistry XXXX, XXX, XXX−XXX

Cryotrapping Spectra. The full cryokinetic spectra and analysis of HhaI PYP were published previously.[59] Here we focus on the excitation-wavelength dependence of the difference spectra at only two temperatures, 90 and 170 K. Upon 405 nm illumination at 90 K, the spectra display a positive I_0 photoproduct band at 500 nm and a possible pUV photoproduct at 375 nm. The ground-state bleach has multiple peaks at 455 and 425 nm and a shoulder at 400 nm (Figure 4A).

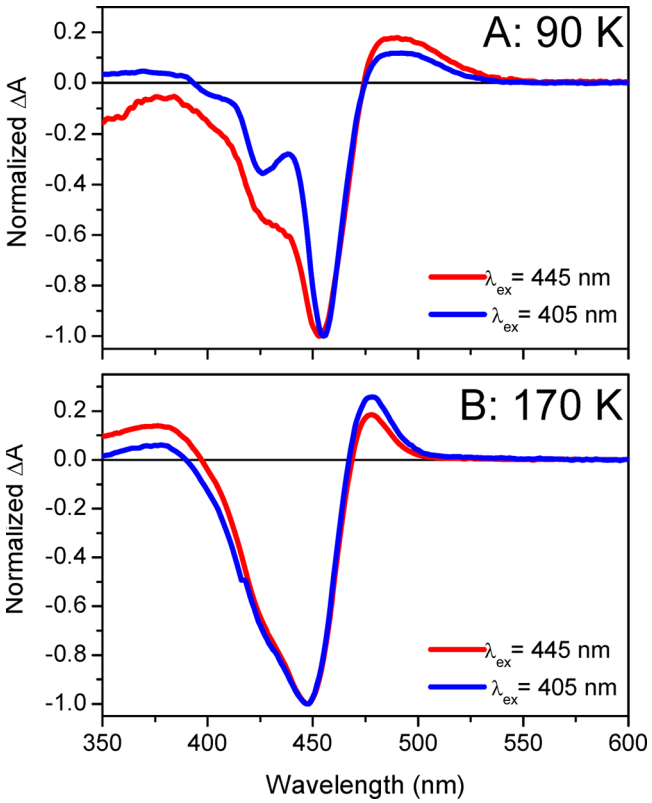

Figure 4. Cyrotrapped spectra at two temperatures [(A) 90 K and (B) 170 K] after illumination with 445 nm light (red curves) and 405 nm light (blue curves). The obvious differences in the I_0 feature at 500 nm and the GSB between the two pump wavelengths at 90 K are not present after evolution of the photocycle at 170 K. Wavelength-dependent processes influence only the early stages of the photocycle.

Immamoto and co-workers[20] also observed multiple GSB signals via low-temperature spectroscopy. Under illumination with a different laser diode at 445 nm and 90 K, I_0 is still present, with no clear pUV state and with altered relative amplitudes of the multiple GSB signals. Illumination with 405 nm light results in weaker I_0 signals and a more intense bleach at 425 nm, while illumination with 445 nm light results in a larger I_0 band with a smaller 425 nm bleach feature. These data indicate that illumination at different wavelengths manipulates subpopulations of the HhaI PYP ground state that cannot interconvert because of the low thermal energy available; 405 nm illumination favors the 425 nm subpopulation and contributes less to I_0 photoproduct formation, while 445 nm illumination favors the 455 nm subpopulation with more I_0 photoproduct formation. Also, 405 nm illumination may favor the 400 nm subpopulation, but the small shoulder does not have sufficient definition in the spectra to make an evaluation. At 90 K, there is a clear wavelength dependence with at least two separate GSB subpopulations and different I_0 evolution.

The photocycle evolves as the temperature is increased to 170 K, and the cryotrapping spectra under each illumination wavelength are now essentially identical. At this temperature, the pR state is beginning to form with a peak at 475 nm and the pUV state at 375 nm is decaying. The GSB still displays some asymmetry with a shoulder at 425 nm, but the shapes of the bleach after 405 nm radiation and that after 445 nm radiation are equal. The initial excitation-wavelength-dependent spectra of the HhaI PYP photocycle are not present at higher temperatures further along the photocycle.

Primary Photodynamics. Both data sets in the DEWI-PP signals produced by 435 and 475 nm excitation exhibit qualitatively similar features as demonstrated previously for WT HhaI PYP.[28,35,49,59] To quantitatively compare the transient dynamics initiated from the two excitation wavelengths, the spectra of both data sets were scaled to the bleach region from 400 to 450 nm in the terminal 6 ns spectrum. The spectra (Figure 5A) of the 435 nm excitation (blue) and 475 nm excitation (red) initially exhibit a ground-state bleach (GSB) between 400 and 475 nm with an excited-state absorption (ESA) in the range of 340−400 nm and a stimulated emission (SE) in the range of 450−600 nm. The ESA and SE signals for the 475 nm excitation are slightly higher, indicating that a greater proportion of the sample was excited with respect to the terminal population amplitude (Figure 5A,B). The GSB in the 475 nm excitation spectra is also noticeably red-shifted compared to the 435 nm excitation spectra at early probe times.

By 60 ps (Figure 5F), the differences in amplitude in the ESA and SE have converged with formation of the I_0 photoproduct; spectra from both excitation wavelengths are nearly identical, including the GSB. This finding agrees with the cryotrapping analysis in which initial differences in GSB spectra with different excitation wavelengths evolve into a single GSB shape. At 1.2 ns, the spectra have diverged as the amplitude of the I_0 state (near 500 nm) is slightly larger upon 475 nm excitation than that for 435 nm excitation (Figure 5G). For the 6 ns spectra (Figure 5H), the GSB signal amplitudes are normalized from 400 to 450 nm, suggesting equal coexisting populations, but with different pR contributions.

Both DEWI-PP signals exhibit triphasic excited-state kinetics (Figure 6), mirroring observations from WT HhaI PYP transient absorption data measured previously.[13,33−35,49,59] The ESA kinetics at 375 nm (Figure 6A) exhibit a greater amplitude after 475 nm excitation (red curve) than after 435 nm excitation (blue curve) for the duration of the experiment. The slight positive signal in the nanosecond regime is likely due to the pUV state recently reported for Hh PYP and other PYPs,[59,70] but this state does not emerge from further global analysis, because of its very low level of accumulation. The 450 nm GSB trace (Figure 6B) exhibits an initial deeper bleach in the 475 nm excitation and the convergence of the two excitation signals around 100 ps. The 510 nm (Figure 6C) and 550 nm (Figure 6D) traces the SE signals decay into a similar positive I_0 signal at ∼10 ps, followed by a decay as I_0 evolves into the blue-shifted pR population at ∼300 ps.

Global Analysis. Multicompartment global analysis techniques were used to quantitatively describe the ultrafast signals for both excitation wavelengths.[84,85] Multiple kinetic models were created and evaluated on the basis of their ability to represent a plausible molecular mechanism, and their simplicity. If a model is the true representation of the mechanism, then the extracted species-associated difference spectra (SADS) are the

DOI: 10.1021/acs.biochem.7b01114
Biochemistry XXXX, XXX, XXX−XXX

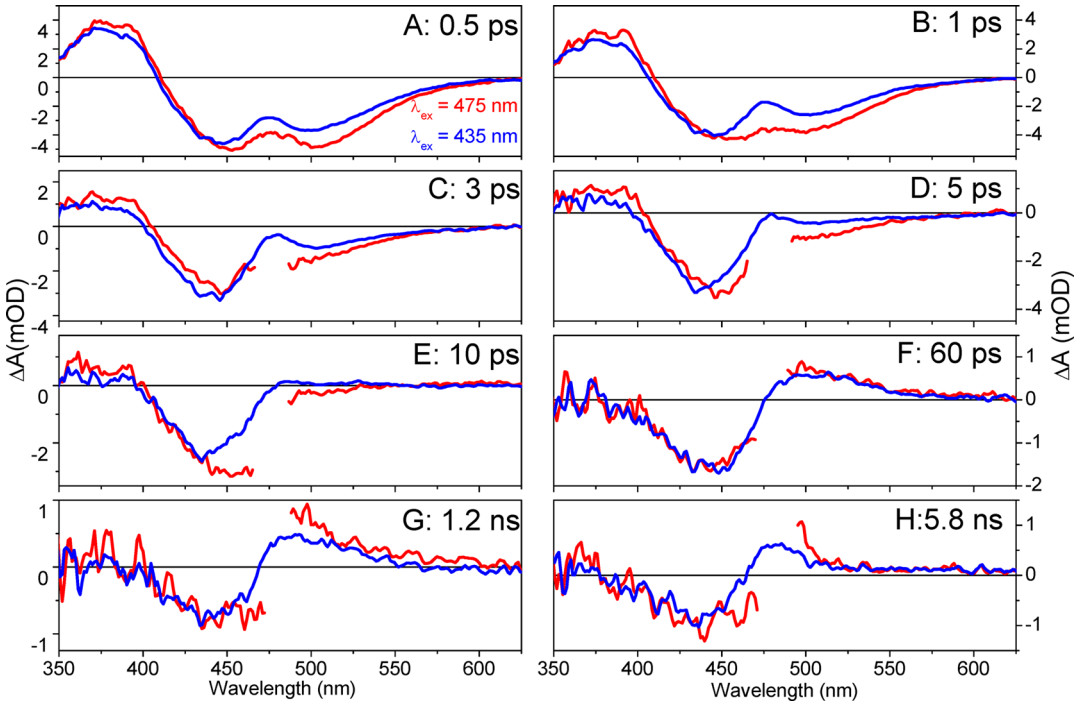

Figure 5. Comparison of select transient spectra from 435 nm excitation (blue) and 475 nm excitation (red) at selected probe times as indicated. Removed regions of the 475 nm excitation spectra are due to excessive pump scattering; the 435 nm data set did not exhibit significant scattering to warrant the excision of data. Panels A and B clearly illustrate the pG* spectra of Hhal PYP with ESA, GSB, and SE signals. Panels C and D show the decay of the pG* state and the red-shifted GSB upon 475 nm excitation. In panels E and F, the I_0 state is formed and blue shifts in panel G into the last observed pR photoproduct in panel H. The spectra were normalized for comparison at 6 ns from 400 to 450 nm.

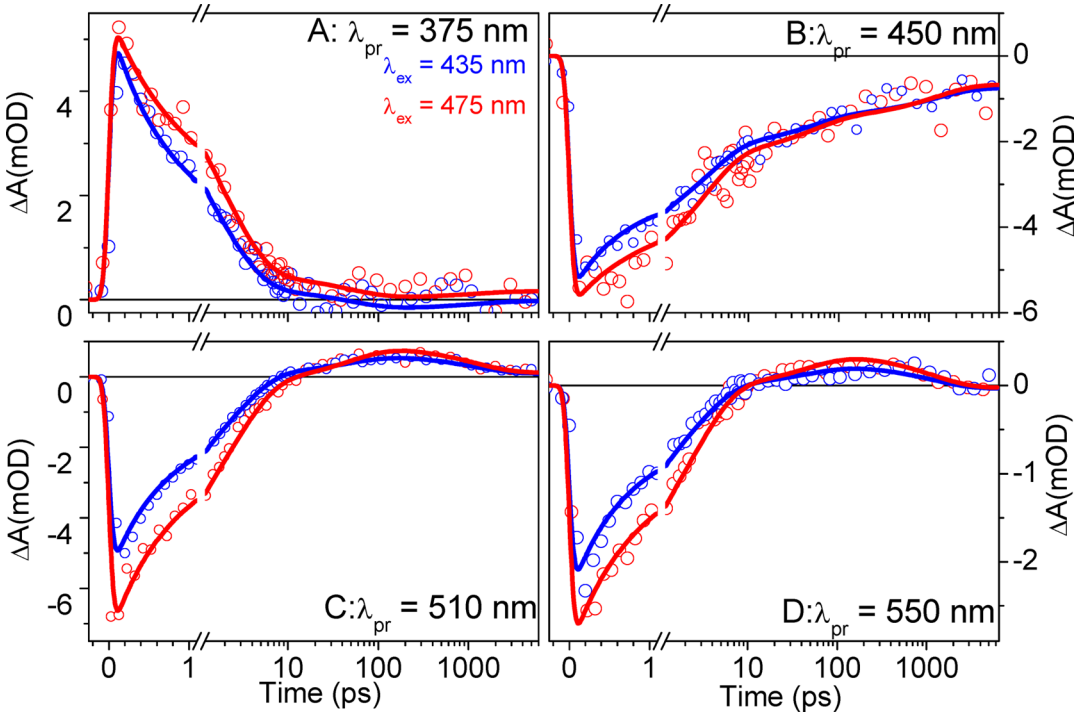

Figure 6. Kinetics (empty circles) for 435 nm excitation (blue) and 475 nm excitation (red) at specific wavelengths with the global analysis fits (line). (A) ESA decay, (B) GSB, (C) evolution from SE to I_0 to pR, and (D) largely SE kinetics with some I_0 influence. As with the spectra in Figure 5, the data were normalized for comparison at 6 ns from 400 to 450 nm. Figures S1 and S3 compare the kinetics across the probed wavelengths.

"correct" spectra of the constituent populations; if a model is inaccurate, the SADS represent a linear combination of the spectra of the real species. In this effort, two models were developed based on models that were developed for PYP previously.[35,49,86,87] The first model (Figure 7) has three heterogeneous ground states that are excited to pG* and may relax into a short-lived ground-state intermediate (GSI) population before returning to the pG ground state or evolve

DOI: 10.1021/acs.biochem.7b01114
Biochemistry XXXX, XXX, XXX−XXX

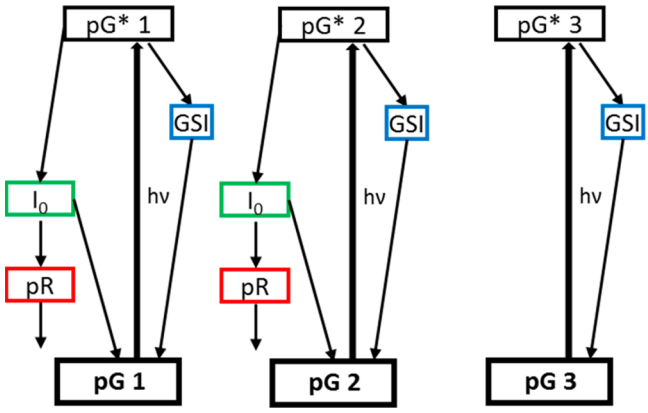

Figure 7. Three-state heterogeneous global analysis model for fitting the transient absorption dynamics from each DEWI-PP data set with different parameters. The excitation-wavelength dependence shows up in the spectral features of the extracted SADS from the fits.

to produce I_0 and pR. The second model (Figure S1B) has two heterogeneous ground states that vibrationally relax and isomerize on comparable time scales.

Both global models fit the dynamics of Hhal PYP excitation nearly identically with root-mean-square fit errors of 0.909 and 0.896 (a difference of 1.4%). In each model, the kinetics at 435 and 475 nm are fitted with the same kinetic parameters and the wavelength-dependent differences are resolved in the corresponding SADS spectra. While both models include inhomogeneity to explain the DEWI-PP data, the three-state heterogeneous model is preferred for its simplicity. Hence, the remainder of the discussion will focus on the application of the three-state inhomogeneity model in Figure 7; however, for the sake of completeness of the discussion, the kinetic parameters and spectra for the two-state vibrational relaxation model are given in Table S2 and Figures S4 and S5.

Within the inhomogeneous model in Figure 7, both DEWI data sets are fit to the same similar triphasic pG* quenching kinetics with 1.1, 4.7, and 34 ps lifetimes (Table 1 and Figure 7, black boxes). As demonstrated below, the DEWI data sets can be fit with the same decay time constants, but with differing amplitudes and spectra. While previous studies[35,48,59] of WT Hhal PYP assumed that each pG* population was spectrally identical with different kinetic time constants, the raw DEWI-PP data in Figures 4 and 5 clearly show that 435 and 475 nm excitations produce similar, albeit not identical, pG* spectra. Thus, the SADS of the constituent pG* states must be different in the modeling. The SADS of the fastest and intermediate pG* populations were unconstrained in the global analysis fitting, while the weak-amplitude third population was locked to the second. The ESA features in all the pG* spectra are identical both among and between excitation wavelengths. In all the pG* GSB features, excitation at 475 nm versus excitation at 435 nm produces a red-shifted bleach by ~10 nm. All the 475 nm excitation pG* states also produce SE signals with amplitudes greater than those of the 435 nm excitation compared to the GSB. This suggests the higher fluorescence yield (Figure 3C) observed after 475 nm excitation versus 435 nm excitation may result in part because of an increased oscillator strength and changing quantum yields. Within a single excitation wavelength, there are slight differences in the SE regions of the different heterogeneous pG* states. Under 435 nm illumination, the pG* 1 SE at 500 nm produces a more rounded gradual peak than at later times in pG* 2 and pG* 3. Under 475 nm illumination, the SE is blue-shifted slightly and forms a sharper peak than in pG* 2 or pG* 3. These differences are more evident when the pG* spectra are overlapped as seen in Figure S3.

Quenching of pG* populations proceeds through a GSI[35] (Figure 8D and Figure 7, blue boxes) that is argued via pump−dump−probe spectroscopy to be a highly vibrationally excited electronic ground-state species that is produced when the *p*CA chromophore fails to enter the photocycle and nonradiatively relaxes.[35] The transient GSI spectra are red-shifted from the GSB peaking at 470 nm. The GSI spectrum with 475 nm excitation clearly shows the red-shifting of the GSB spectra at early times compared to the 435 nm excitation GSB.

The DEWI-PP data indicate that the heterogeneity of the excited-state pG* populations may not propagate through the first two intermediates of the resulting photocycle dynamics. The I_0 (Figure 8E) state exhibits slight kinetic and spectral differences depending on the excitation wavelengths, but the main indicator of heterogeneity, the GSB, is almost identical. The recombination of the bleach spectra at later probe times matches the results of the cryotrapping experiments that showed the GSB differences also recombined at higher temperatures (Figure 4). The pR SADS (Figure 8F) with 475 nm excitation do produce a slightly larger bleach at the peak; however, the GSB region as a whole is similar.

The photoproduct quantum yields (Φ_{ph}) were evaluated from the populations and branching ratios modeled in our global analysis (Table 1). In agreement with previous PYP studies,[35,49,59,87] the overall pR yield is 22% and the primary contributor to the production of I_o and pR is the fastest pG* 1 state. Because both excitation wavelengths are fit to the same model to make the spectral differences clear, we did not calculate any differences in the quantum yield under 435 or 475 nm excitation.

Table 1. Global Analysis Parameters of the DEWI Data Sets[a]

	Heterogeneous Model					
	pG* 1	pG* 2	pG* 3	GSI	I_0	pR
population (%)	57	32	11			
lifetime (ps)	1.1	4.7	34	4.5	970	∞
branching	67 (GSI)	67 (GSI)	100 (GSI)		35 (pG)	
yield (%)	33 (I_0)	33 (I_0)	0 (I_0)		65 (pR)	
pR yield (%)	14	8	0			total of 22

[a]These are optimized by target analysis to the model in Figure 7 for Hhal PYP after 435 and 475 nm excitation. The relative error for each parameter is 10%.

DOI: 10.1021/acs.biochem.7b01114
Biochemistry XXXX, XXX, XXX−XXX

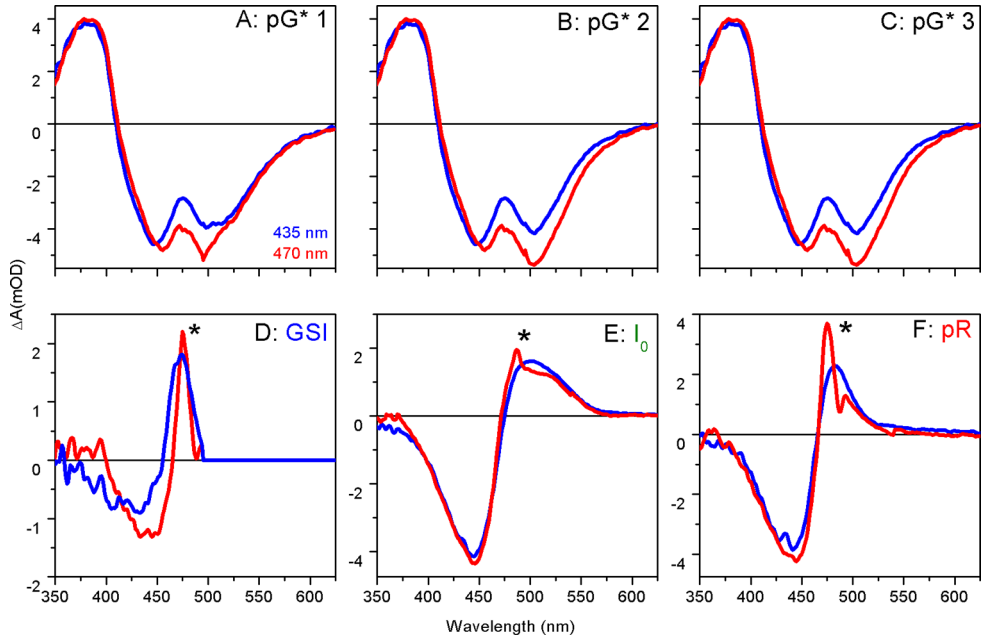

Figure 8. Comparison of global analysis SADS for 435 nm excitation (blue) and 475 nm excitation (red). Spectra are calculated from the transient absorption spectra that were normalized at 6 ns between 400 and 450 nm. The target model and concentration profiles correlated with these SADS are shown in Figure 7. Panels A–C show the SADS for the three heterogeneous pG* states. In panels B and C, the red shift of the GSB with 475 nm excitation is evident. The GSI spectra and the extremely clear difference in the GSB at early times are shown in panel D. The I_0 intermediate SADS are shown in panel E and the later pR photoproduct SADS in panel F, where the GSBs are approximately identical. The sharp peaks (denoted with asterisks) in panels D–F are due to scattering of the 475 nm excitation light into the detector.

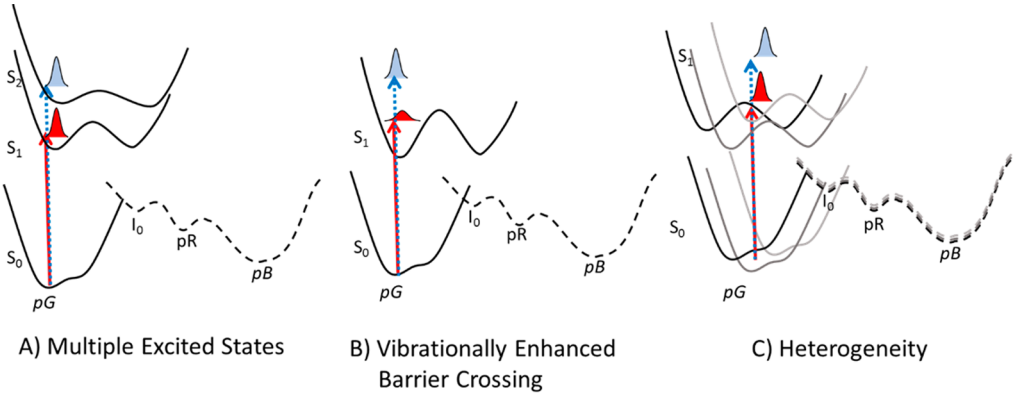

Figure 9. Depiction of three models conceived to explain excitation-wavelength dependence in PYP: (A) multiple-electronic excited-state model, (B) vibrationally enhanced isomerization model, and (C) static heterogeneity model.

DISCUSSION

While the differences between 435 and 475 nm excitation are small, they are well-resolved in the DEWI-PP measurements. The primary photodynamics, cryotrapping spectra, and fluorescence dynamics of PYP are clearly manipulated by excitation wavelength. Three hypotheses are considered for the origin of this effect (Figure 9): (1) the multiple-electronic excited-state model, (2) the vibrationally enhanced isomerization model, and (3) the static heterogeneity model.

Multiple-Electronic Excited-State Model. This model hypothesizes that the pG spectrum of HhaI PYP is attributed to a single homogeneous population with two or more overlapping absorption bands attributed to different electronic transitions (Figure 9A). Excitation to different excited-state potential energy surfaces will affect the nature of the intersections with the ground state, leading to different photodynamics. Other photochemical systems like azobenzene[88] and metal carbonyls[89] are known examples of multiple electronic excited states that influence photochemistry.

If excitation into different excited electronic states of PYP (Figure 9A) resulted in differing photodynamics, then the fluorescence, cyrotrapping, and DEWI signals would certainly exhibit an excitation-wavelength dependence. Quantum calculations[90,91] that include the local amino acid environment predict a large energy gap (≥1 eV) between S_1 ($\pi \rightarrow \pi^*$) and S_2 ($n \rightarrow \pi^*$) that places the $n \rightarrow \pi^*$ transition out of reach of the wavelengths in this DEWI-PP experiment (435 nm, 2.8 eV; 475 nm, 2.6 eV). There is evidence of multiple excited states influencing the isomerization of the neutral pCA chromophore in the gas phase,[92] but subsequent efforts have called this result into question.[93]

Multiple excited states are consistent with some aspects of the HhaI PYP dynamics. The observed fluorescence spectra exhibit red shifting with excitation wavelength (Figure 3B),

DOI: 10.1021/acs.biochem.7b01114
Biochemistry XXXX, XXX, XXX−XXX

consistent with multiple excited states in which excitation on the red edge excites a pG* state at a lower energy. The gradual fluorescence peak shift opposed to a large discrete jump requires multiple pG* populations close in energy. In the DEWI-PP measurements, differences between the triphasic pG* decay at different excitation wavelengths can be interpreted using three pG* states. Each of the multiple pG* states has its own spectral form and decay constants for the transition to the ground state.

The multiple-excited-state model additionally predicts a homogeneous single GSB that is independent of excitation wavelength. This is inconsistent, however, with the multiple bleach subpopulations observed in the cryotrapping spectra and ultrafast transient absorption experiments. At low temperatures, excitation at 405 nm produces an obvious shifts toward a 425 nm bleach subpopulation compared to that seen upon excitation at 445 nm (Figure 4). In the ultrafast experiments, 435 nm excitation produces a blue-shifted bleach while 475 nm excitation produces a red-shifted bleach. Hence, while this hypothesis can explain the pG* triphasic decay and fluorescence emission, it is not sufficient for the wavelength-dependent behavior of the GSB.

Vibrationally Enhanced Isomerization Model. This model postulates that the photoisomerization behavior of Hhal PYP is ascribed to a homogeneous population with an electronic excited-state manifold with multiple vibronic levels that result in differing isomerization dynamics (Figure 9B). Photoexcitation launches a wave packet on this potential energy surface based on the amount of vibrational energy deposited by excitation (above the 0−1 transition energy). The excitation-wavelength dependence of stilbene photoisomerization is heavily influenced by vibrational motion along the isomerization coordinate[94] increasing the rate and quantum yield in solution compared to those in the gas phase. The barrierless isomerization in rhodopsin is also dependent on wavelength because of excited-state vibrational wave packets,[95] with a significant drop in yields above 500 nm. For a vibrationally enhanced isomerization model to significantly affect the isomerization dynamics, the time scale of photoproduct formation must be comparable to that of vibrational relaxation. Because of the relatively short dephasing time of <1 ps, here, only the fastest decay component could be modulated due to vibrational enhancement.

If Hhal PYP is influenced by purely vibrationally enhanced barrier crossing, higher-energy excitation should have significant effects on the photodynamics by allowing easier barrier crossing to produce faster excited-state kinetics, greater photoproduct yields, and less fluorescence. Excitation at shorter wavelengths and higher vibrational energies are predicted to produce higher photoproduct yields and lower fluorescence, and longer wavelengths with lower vibrational energies to produce lower photoproduct yields and higher fluorescence. GSB and photoproduct spectra and kinetics should be identical regardless of the excitation wavelength in the vibrational enhanced barrier crossing model with a single ground-state potential surface.

The observed fluorescence, cryotrapping, and transient spectra all deviate from the predictions by a pure vibrationally enhanced barrier crossing model. The curious shape of the fluorescence quantum yields (Figure 3C) with a minimum at 440 nm and maxima at 400 and 475 nm is not consistent with the steady increase in fluorescence at longer wavelengths predicted by a vibrational enhancement model. As with the multiple-excited-state model, the obvious differences in the GSB and photoproduct spectra are not consistent with a single ground state. For the red-shifted bleach under 475 nm excitation to be the result of only Stokes shifting, the vibrational relaxation time would need to be around 100 ps, which is implausibly slow. Stokes shifting may be responsible for the red shift in the SE band at early times (Figure 5A,B), but any differences in the GSB bleach caused by the Stokes shift would not persist later in the experiment. Furthermore, at 90 K, the thermal energy available to produce vibrational effects is greatly decreased and at least two obvious ground-state subpopulations are observed in the cryotrapping spectra. As with the multiple-excited-state model, vibrationally enhanced barrier crossing can explain some aspects of the pG* kinetics and quantum yields of the wavelength dependence but not the wavelength-dependent ground-state bleach.

Static Heterogeneity Model. This model argues that the absorption spectrum of Hhal PYP can be ascribed to a single S_1 excited state, but that multiple subpopulations coexist because of functionally relevant variations in the protein environment (Figure 9C). The heterogeneous mechanism predicts that the primary photochemistry varies with excitation wavelength because it is possible to selectively excite different subpopulations that exhibit differing intrinsic photodynamics.

The static heterogeneous model combines features of multiple pG* excited states with multiple ground states. In the heterogeneous system, each ground state and each excited state can have a different potential energy surface with a different energy separation and different fluorescence spectra. The wavelength dependence in both the Hhal PYP fluorescence emission spectra and fluorescence quantum yield (Figure 3) indicate that excitations at 400, 446, and 480 nm are sampling different portions of the pG* surface with different local minima and different fluorescence energies. The first pG* subpopulation exhibits a relatively high fluorescence quantum yield (near 0.3%) and a relatively blue-shifted emission spectrum peak near 491 nm; the second subpopulation has a lower fluorescence quantum yield and an emission peak near 492 nm, and the third subpopulation has a somewhat higher fluorescence quantum yield combined with a red-shifted emission spectrum near 498 nm.

Cryotrapping spectra also support a heterogeneous model with two obvious subpopulations and a possible third. These subpopulations are evident at 90 K (Figure 4A) where the ground-state bleach has two peaks at 455 and 425 nm and a possible shoulder at 400 nm. With a change in the excitation wavelength, the occupation of these ground-state subpopulations and their influence on the initial I_0 photoproduct can be manipulated. Excitation at 445 nm results in a smaller 425 nm bleach and a larger I_0 amplitude, implying that most of the photoproduct is formed by the 455 nm ground state.

The transient spectra in the DEWI data sets (Figures 5 and 6) are also consistent with a three-state heterogeneous model. Transient spectra display multiple pG* states with different spectra and kinetic properties. The triphasic decay kinetics are best fit by a linear combination of three exponential rates, representing the three heterogeneous pG* states. These pG* states also display spectral differences with the fastest population having different SE features. Heterogeneity also provides the best framework for interpreting the wavelength-dependent differences in the GSB and the photoproduct spectra. Excitation with 475 nm light on the red edge of the absorption spectra preferentially excites the reddest heteroge-

DOI: 10.1021/acs.biochem.7b01114
Biochemistry XXXX, XXX, XXX−XXX

neous population, resulting in red-shifted GSB spectra compared to those seen with 435 nm excitation.

The second model developed for PYP (Figure S1B) is a hybrid of the vibrational enhanced isomerization and static heterogeneity. The static heterogeneity is responsible for the shifts in the GSB, and the vibrational relaxation contributes to the fit of the shifting SE signals observed at early times of <10 ps (Figures S4 and S5). Attempts to assign the shifted GSB to the vibrational relaxation were not fruitful, and any model explaining the GSB required heterogeneity. Vibrational relaxation may have a place in the dynamics of Hhal PYP, but it is incapable of explaining all the observed wavelength dependence alone without the inclusion of heterogeneity. Heterogeneity is the simplest hypothesis available consistent with triphasic pG* decay, and wavelength-dependent GSB bleaches.

Adoption of a heterogeneous model can explain aspects of the Hhal PYP photodynamics other studies have explained with more complicated models. Models with bifurcation[20,52] following pG* to produce two different photoproducts can be expressed using two heterogeneous states each producing their unique product. Each heterogeneous pG* state has unique kinetic and spectral properties, and they can produce varied photoproducts without bifurcation. Models with equilibria[51] can also be redrawn using heterogeneous states. Equilibria are mainly used to allow the production of primary photoproducts later in the photocycle. With heterogeneous states, primary photoproducts can be produced at different time scales in each pG* state. This allows for the production of a photoproduct over an extended period of time without introducing equilibria. We believe that the heterogeneous model is the appropriate explanation for the Hhal PYP photodynamics.

Heterogeneity in PYP. Heterogeneous Hhal PYP populations are likely created by variations in the positioning of the protein scaffold around the *p*CA chromophore.[96] Proteins are not static objects, and in solution at physiological temperatures, they are dynamic, continually flexing and rotating to sample different portions of the ground potential energy surface.[97] Variations in the hydrogen bonding network of the reversibly switchable fluorescent protein Dronpa[98] demonstrate structural heterogeneity can be a key element in protein photocycles. The origins of the observed heterogeneity in Hhal PYP have been examined by computational and nuclear magnetic resonance (NMR) experiments exploring the conformations of R52 and T50 with respect to the *p*CA chromophore as potential heterogeneous agents.

R52 is in the chromophore binding pocket and shields *p*CA from solvent exposure in the folded pG state. The positive charge of arginine has been proposed to provide a counterion to the negative charge of the deprotonated chromophore, with a significant influence on the electronic potential energy surface of *p*CA and the subsequent excited-state dynamics.[99,100] The charge of the R52 residue remains a subject of controversy as multiple structural studies have produced conflicting results. Yamaguchi et al.[71] observed a neutral charge in their neutron diffraction studies; earlier neutron diffraction studies by Moffat and co-workers[101] did not, and the most recent crystallography effort by Kataoka[102] argues for both the cationic and neutral forms. The NMR titration results of Mulder and co-workers posit that R52 is protonated in solution, which is probably more relevant to the *in vivo* action of Hhal PYP than crystals.[103] Further support for a protonated R52 in the crystal comes from computer simulations that predicted an increase in pK_a rather than a decrease in R52 pK_a in crystals.[104]

The R52Q mutant exhibits slower excited-state dynamics[105−107] and a photocycle quantum yield ∼10% lower than that of PYP (21%[108] vs 25−35%), while the absorption spectrum is nearly identical to the WT spectrum (446 nm). Solution NMR structures of the pG state place R52 in two configurations: either with the guanidinium group positioned directly above the phenol ring of *p*CA or alternately with the guanidinium group positioned far from *p*CA and above Y98.[109] QM/MM calculations by Groenhof and co-workers[110] predict the guanidinium group is oriented either perpendicular or parallel to the *p*CA ring with a difference of ≲20 nm in the absorption spectra of pG based on the orientation. Further calculations using the Gromos96 force field solidify the influence of different conformers of R52 on the photocycle.[99,110,111]

New calculations using the Amber03 force field, presented here, have arrived at other possible conformers of R52 (Figure 10 and Table 2). In the majority of the dynamics simulations,

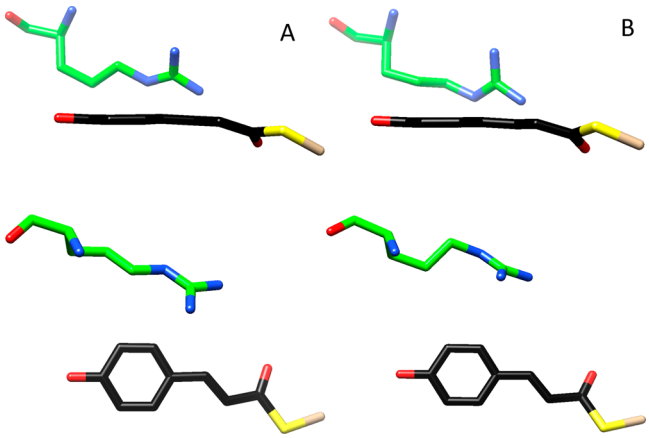

Figure 10. The (A) 60° and (B) −60° conformers of R52 (green) from calculations using the Amber3 force field in relation to the pCA chromophore (black) in the ground pG state.

Table 2. Possible Heterogeneous Conformers of PYP Revealed by QM/MM Simulations

	R52[a]		T50[a]		
	60	−60	Y42	E46	*p*CA
occupation percentage (%)	97	3	12	10	78
estimated lifetime	15 ns	160 ps	13 ps	14 ps	40 ps
vertical electronic excitation (nm)	454	439	423	453	426

[a]See Figures 9 and 10 for structures.

R52 is observed in the perpendicular conformer with a torsion angle of 60° (Figure 10A), similar to the X-ray structure determined by Yamaguchi et al.[71] The R52 residue also samples a configuration with a torsion angle of −60° (Figure 10B), in line with the NMR structure determined by Bernard et al.,[112] and rarely appears in the parallel conformer seen in the previous calculations.[110] Although the −60° R52 conformer is less populated than the 60° conformer, there are several transitions, and the −60° conformation has a lifetime that is significantly longer than the excited-state lifetime of the chromophore (Table 2). The 60° and −60° conformers display differences in their electronic excitations with absorption at 454

DOI: 10.1021/acs.biochem.7b01114
Biochemistry XXXX, XXX, XXX−XXX

and 439 nm (Table 2). Despite the differences in relative populations of the various R52 conformations, in simulations with both force fields, the WT PYP undergoes the transition from *trans*-*p*CA to *cis*-*p*CA along identical pathways.[60] All of these conformers of R52 are qualitatively valid options for the positioning in the chromophore pocket and one mechanism that may be responsible for the heterogeneous dynamics resolved in the fluorescence, cryotrapping, and DEWI data of Hhal PYP photodynamics.

T50 has also been identified as a possible source of heterogeneity in the chromophore pocket of Hhal PYP. The T50 residue is an important member of the hydrogen bonding network around the phenolate end of the pCA chromophore, and any variations in its positioning would strongly influence the photodynamics. Crystallography and neutron diffraction results place T50 with a hydrogen bond to Y42 (Figure 11A).

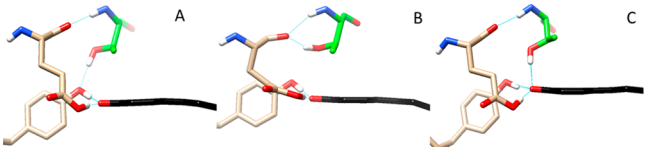

Figure 11. Three different conformers of T50 (green) in relation to the hydrogen bonding network around the pCA chromophore (black) in the ground pG state. In panel A, the T50 residue bonds with the Y42 alcohol (background). In panel B, the T50 residue bonds with the E46 backbone carbonyl (foreground). In panel C, the T50 residue bonds with *p*CA (black).

Computations performed by Ochsenfeld and co-workers[113] and confirmed in this work, demonstrate that T50 samples three different orientations with different hydrogen bond networks. First, T50 may hydrogen bond to Y42 as seen in the crystal structures (Figure 11A). Second, T50 may hydrogen bond to the carbonyl on the E46 backbone (Figure 11B). Third, T50 may hydrogen bond directly to the phenol of the *p*CA chromophore (Figure 11C). Ochsenfeld and co-workers[113] used these three conformers to calculate an accurate chemical shift for the E46 proton. In our simulations, these three conformers exchange on a picosecond time scale and have different electronic transitions. The T50−Y42 conformer undergoes a transition at 423 nm, the T50−E46 backbone conformer at 453 nm, and the T50−*p*CA conformer at 426 nm (Table 2).

Although these shifts are in line with the single configurational approximate coupled-cluster calculations of Ochsenfeld and co-workers,[113] our multiconfigurational perturbation results suggest that the main absorption in solution is due to the configuration in which T50 is hydrogen bonded with the E46 backbone (Figure 11B and Table 2). Excitation-wavelength-dependent excited-state populations would be expected in Hhal PYP based on the T50 conformer population distribution at the moment of absorption. Collectively, the variations in the calculated positions of T50 and R52 provide compelling evidence that there are ample degrees of freedom in the Hhal PYP chromophore pocket to produce excitation-wavelength-dependent heterogeneous ground states, excited states, and photoproducts.

Regardless of the origin, the wavelength-dependent heterogeneous Hhal PYP photodynamics requires reevaluation of the literature. Prior works paid little attention to the possible effect of wavelength dependence and the ability to compare experiments performed with different illumination wavelengths. It is expected that a range of excitation wavelengths greater than the range of 40 nm used in this study (Figure 2) would reveal more profound differences in the associated dynamics. Time-resolved crystallography by Anfinrud and co-workers[51] with a 390 nm pump should be compared with reservations to crystallography by Ihee and co-workers[52] with an excitation pump at 418 nm and crystallography by Hutchinson and van Thor[114] with an excitation pump at 450 nm. Because any bulk sample represents a weighted average over all possible heterogeneous structures, different excitation wavelengths among the time-resolved crystallographic structures[51,52,57,60] create a different distribution of excited heterogeneous populations whose spectral, kinetic, quantum yield, and structural properties are not equivalent. This same argument applies to any comparisons of techniques using different pump wavelengths (Figure 2 and Table S1), including low-temperature spectroscopy,[15,20,56,59] visible ultrafast transient experiments,[49,59,87,115] infrared observations,[29,32] and fluorescence measurements.[21,31,116] Direct comparisons of PYP studies that have been performed using dissimilar pump wavelengths must be performed with caution and are not expected to yield identical kinetic lifetimes or spectra.

Concluding Comments. Wavelength-dependent excitation of Hhal PYP with 475 nm light versus 435 nm light has a small, but measurable, effect on the fluorescence, cryotrapped spectra, and ultrafast photodynamics. We would expect these effects to scale with excitation far from the 440 nm absorbance center to display the greatest deviations. Multiple excited-state interactions, vibrationally enhanced barrier crossing, and pG heterogeneity are possible causes of the wavelength dependence. Heterogeneity in the ground, excited, and photoproduct states is the only model that can explain all of the differences, including the ground-state bleaches, triphasic excited-state quenching, photoproduct amplitudes, and quantum yields. Heterogeneity is likely created by the subtle movements of proteins in solution environments, and PYP rotamers of R52 are a possible contributor. Conformers of T50 resulting in variations of the hydrogen bond network have also been identified in new QM/MM calculations as possible heterogeneous residues. Confirmation of wavelength dependence in PYP encourages researchers to use caution with all future and past comparisons between PYP studies with different excitation wavelengths.

■ ASSOCIATED CONTENT

Supporting Information

The Supporting Information is available free of charge on the ACS Publications website at DOI: 10.1021/acs.biochem.7b01114.

Additional information, Tables S1 and S2, Figures S1−S5, and additional references (PDF)

■ AUTHOR INFORMATION

Corresponding Authors

*E-mail: dlarsen@ucdavis.edu.
*E-mail: wouter.hoff@okstate.edu.

ORCID

Wendy Ryan Gordon: 0000-0001-7696-5560
Delmar S. Larsen: 0000-0003-4522-2689

Present Addresses

[@]E.C.C.: Department of Imaging Physics, Delft University of Technology, Lorentzweg 1, 2628 CJ Delft, The Netherlands.

DOI: 10.1021/acs.biochem.7b01114
Biochemistry XXXX, XXX, XXX−XXX

▽J.P.: Department of Physics, Florida International University, Modesto A. Maidique Campus, 11200 SW 8th St., ECS 450, Miami, FL 33199.
●W.R.G.: Department of Biochemistry, Molecular Biology and Biophysics, The University of Minnesota, Twin Cities, 6-155 Jackson Hall, 321 Church St. SE, Minneapolis, MN 55455.
○A.P.: Genesis Health System, 1227 E. Rusholme St., Davenport, IA 52803.
■M.K.: Strategic Core research Center, Sanshin Metal Working Co., Ltd, 2-9-9 Niihama, Tadaoka-cho, Senboku-gun, Osaka 595-0814, Japan.

Funding
This work was supported by a grant from the National Science Foundation (CHE-1413739) to both D.S.L. and W.D.H. Additionally, W.D.H. acknowledges additional support from National Science Foundation Grants MCB-1051590 and MRI-1338097. G.G. and D.M. acknowledge support from the Academy of Finland (Grants 258806, 290677, and 304455 to G.G. and Grant 285481 to D.M.). The authors also acknowledge CSC-IT Center for Science, Finland, for computational resources.

Notes
The authors declare no competing financial interest.

■ ACKNOWLEDGMENTS

Dr. Mikas Vengris (Light Conversion Ltd.) is acknowledged for the donation of the global and target analysis software package used initially in the analysis.

■ ABBREVIATIONS

PYP, photoactive yellow protein; Hhal, *H. halophila*; WT, wild type; *p*CA, *p*-coumaric acid; PAS, Per-Arnt-Sim; BLUF, blue light using FAD; FAD, flavin adenine dinucleotide; LOV, light-oxygen-voltage; fwhm, full width at half-maximum; NOPA, nonlinear optical parametric amplifier; TA, transient absorption; GROMACS, Groningen MAchine for Chemical Simulation; TIP3P, transferable intermolecular potential with 3 points; *NPT*, constant *N*, constant pressure, and constant temperature; GAMESS(US), General Atomic and Molecular Electronic Structure System U.S. variant; VEE, vertical excitation energy; XMCQDPT2, extended multi-monfigurational quasi-degenerated perturbation theory; CASSCF, complete active space self-consistent field; S/N, signal to noise ratio; PP, pump−probe; QM/MM, quantum mechanics/molecular mechanics; GSB, ground-state bleach; ESA, excited-state absorption; SE, stimulated emission; GSI, ground-state intermediate; EADS, evolution-associated difference spectra; SADS, species-associated difference spectra.

■ REFERENCES

(1) Kumauchi, M., Hara, M. T., Stalcup, P., Xie, A., and Hoff, W. D. (2008) Identification of Six New Photoactive Yellow Proteins—Diversity and Structure−Function Relationships in a Bacterial Blue Light Photoreceptor. *Photochem. Photobiol. 84*, 956−969.
(2) Meyer, T. E., Kyndt, J. A., Memmi, S., Moser, T., Colon-Acevedo, B., Devreese, B., and Van Beeumen, J. J. (2012) The growing family of photoactive yellow proteins and their presumed functional roles. *Photochemical & Photobiological Sciences 11*, 1495−1514.
(3) Hoff, W. D., Dux, P., Hard, K., Devreese, B., Nugteren-Roodzant, I. M., Crielaard, W., Boelens, R., Kaptein, R., Van Beeumen, J., and Hellingwerf, K. J. (1994) Thiol ester-linked p-coumaric acid as a new photoactive prosthetic group in a protein with rhodopsin-like photochemistry. *Biochemistry 33*, 13959−13962.
(4) Sprenger, W. W., Hoff, W. D., Armitage, J. P., and Hellingwerf, K. J. (1993) The eubacterium *Ectothiorhodospira halophila* is negatively phototactic, with a wavelength dependence that fits the absorption spectrum of the photoactive yellow protein. *J. Bacteriol. 175*, 3096−3104.
(5) Horst, M. A. v. d., Stalcup, T. P., Kaledhonkar, S., Kumauchi, M., Hara, M., Xie, A., Hellingwerf, K. J., and Hoff, W. D. (2009) Locked Chromophore Analogs Reveal That Photoactive Yellow Protein Regulates Biofilm Formation in the Deep Sea Bacterium *Idiomarina loihiensis*. *J. Am. Chem. Soc. 131*, 17443−17451.
(6) Kumar, A., Ali, A. M., and Woolley, G. A. (2015) Photo-control of DNA binding by an engrailed homeodomain-photoactive yellow protein hybrid. *Photochemical & Photobiological Sciences 14*, 1729−1736.
(7) Reis, J. M., and Woolley, G. A. (2016) Photo Control of Protein Function Using Photoactive Yellow Protein. In *Optogenetics: Methods and Protocols* (Kianianmomeni, A., Ed.) pp 79−92, Springer, New York.
(8) Deisseroth, K. (2011) Optogenetics. *Nat. Methods 8*, 26−29.
(9) Müller, K., and Weber, W. (2013) Optogenetic tools for mammalian systems. *Mol. BioSyst. 9*, 596−608.
(10) Meyer, T. E., Yakali, E., Cusanovich, M. A., and Tollin, G. (1987) Properties of a water-soluble, yellow protein isolated from a halophilic phototrophic bacterium that has photochemical activity analogous to sensory rhodopsin. *Biochemistry 26*, 418−423.
(11) Cusanovich, M. A., and Meyer, T. E. (2003) Photoactive Yellow Protein: A Prototypic PAS Domain Sensory Protein and Development of a Common Signaling Mechanism. *Biochemistry 42*, 4759−4770.
(12) Hellingwerf, K. J., Hendriks, J., and Gensch, T. (2003) Photoactive Yellow Protein, A New Type of Photoreceptor Protein: Will This "Yellow Lab" Bring Us Where We Want to Go? *J. Phys. Chem. A 107*, 1082−1094.
(13) Ujj, L., Devanathan, S., Meyer, T. E., Cusanovich, M. A., Tollin, G., and Atkinson, G. H. (1998) New Photocycle Intermediates in the Photoactive Yellow Protein from *Ectothiorhodospira halophila*: Pico-second Transient Absorption Spectroscopy. *Biophys. J. 75*, 406−412.
(14) Brudler, R., Rammelsberg, R., Woo, T. T., Getzoff, E. D., and Gerwert, K. (2001) Structure of the I1 early intermediate of photoactive yellow protein by FTIR spectroscopy. *Nat. Struct. Biol. 8*, 265−270.
(15) Xie, A., Kelemen, L., Hendriks, J., White, B. J., Hellingwerf, K. J., and Hoff, W. D. (2001) Formation of a New Buried Charge Drives a Large-Amplitude Protein Quake in Photoreceptor Activation. *Biochemistry 40*, 1510−1517.
(16) Pan, D., Philip, A., Hoff, W. D., and Mathies, R. A. (2004) Time-Resolved Resonance Raman Structural Studies of the pB′ Intermediate in the Photocycle of Photoactive Yellow Protein. *Biophys. J. 86*, 2374−2382.
(17) Hellingwerf, K. J., Hendriks, J., and Gensch, T. (2002) On the Configurational and Conformational Changes in Photoactive Yellow Protein that Leads to Signal Generation in *Ectothiorhodospira halophila*. *J. Biol. Phys. 28*, 395−412.
(18) Hoff, W. D., Kwa, S. L. S., van Grondelle, R., and Hellingwerf, K. J. (1992) Low-Temperature Absorbency And Fluorescence Spectroscopy of the Photoactive Yellow Protein from *Ectothiorhodospira halophila*. *Photochem. Photobiol. 56*, 529−539.
(19) van Brederode, M. E., Gensch, T., Hoff, W. D., Hellingwerf, K. J., and Braslavsky, S. E. (1995) Photoinduced volume change and energy storage associated with the early transformations of the photoactive yellow protein from Ectothiorhodospira halophila. *Biophys. J. 68*, 1101−1109.
(20) Imamoto, Y., Kataoka, M., and Tokunaga, F. (1996) Photoreaction Cycle of Photoactive Yellow Protein from *Ectothiorhodospira halophila* Studied by Low-Temperature Spectroscopy. *Biochemistry 35*, 14047−14053.
(21) Chosrowjan, H., Mataga, N., Nakashima, N., Imamoto, Y., and Tokunaga, F. (1997) Femtosecond-picosecond fluorescence studies on excited state dynamics of photoactive yellow protein from *Ectothiorhodospira halophila*. *Chem. Phys. Lett. 270*, 267−272.

DOI: 10.1021/acs.biochem.7b01114
Biochemistry XXXX, XXX, XXX−XXX

(22) Genick, U. K., Borgstahl, G. E. O., Ng, K., Ren, Z., Pradervand, C., Burke, P. M., Šrajer, V., Teng, T.-Y., Schildkamp, W., McRee, D. E., Moffat, K., and Getzoff, E. D. (1997) Structure of a Protein Photocycle Intermediate by Millisecond Time-Resolved Crystallography. *Science 275*, 1471−1475.
(23) Chosrowjan, H., Mataga, N., Shibata, Y., Imamoto, Y., and Tokunaga, F. (1998) Environmental Effects on the Femtosecond−Picosecond Fluorescence Dynamics of Photoactive Yellow Protein: Chromophores in Aqueous Solutions and in Protein Nanospaces Modified by Site-Directed Mutagenesis. *J. Phys. Chem. B 102*, 7695−7698.
(24) Devanathan, S., Pacheco, A., Ujj, L., Cusanovich, M., Tollin, G., Lin, S., and Woodbury, N. (1999) Femtosecond spectroscopic observations of initial intermediates in the photocycle of the photoactive yellow protein from *Ectothiorhodospira halophila*. *Biophys. J. 77*, 1017−1023.
(25) Masciangioli, T., Devanathan, S., Cusanovich, M. A., Tollin, G., and El-Sayed, M. A. (2000) Probing the primary event in the photocycle of photoactive yellow protein using photochemical hole-burning technique. *Photochem. Photobiol. 72*, 639−644.
(26) Mataga, N., Chosrowjan, H., Shibata, Y., Imamoto, Y., and Tokunaga, F. (2000) Effects of Modification of Protein Nanospace Structure and Change of Temperature on the Femtosecond to Picosecond Fluorescence Dynamics of Photoactive Yellow Protein. *J. Phys. Chem. B 104*, 5191−5199.
(27) Hanada, H., Kanematsu, Y., Kinoshita, S., Kumauchi, M., Sasaki, J., and Tokunaga, F. (2001) Ultrafast fluorescence spectroscopy of photoactive yellow protein. *J. Lumin. 94−95*, 593−596.
(28) Imamoto, Y., Kataoka, M., Tokunaga, F., Asahi, T., and Masuhara, H. (2001) Primary Photoreaction of Photactive Yellow Protein Studied by Subpicosecond-Nanosecond Spectroscopy. *Biochemistry 40*, 6047−6052.
(29) Imamoto, Y., Shirahige, Y., Tokunaga, F., Kinoshita, T., Yoshihara, K., and Kataoka, M. (2001) Low-Temperature Fourier Transform Infrared Spectroscopy of Photoactive Yellow Protein. *Biochemistry 40*, 8997−9004.
(30) Gensch, T., Gradinaru, C. C., van Stokkum, I. H. M., Hendriks, J., Hellingwerf, K., and van Grondelle, R. (2002) The Primary photoreaction of photoactive yellow protein (PYP): anisotropy changes and excitation wavelength dependence. *Chem. Phys. Lett. 356*, 347.
(31) Mataga, N., Chosrowjan, H., Shibata, Y., Imamoto, Y., Kataoka, M., and Tokunaga, F. (2002) Ultrafast photoinduced reaction dynamics of photoactive yellow protein (PYP): observation of coherent oscillations in the femtosecond fluorescence decay dynamics. *Chem. Phys. Lett. 352*, 220−225.
(32) Groot, M. L., van Wilderen, L. J. G. W., Larsen, D. S., van der Horst, M. A., van Stokkum, I. H. M., Hellingwerf, K. J., and van Grondelle, R. (2003) Initial Steps of Signal Generation in Photoactive Yellow Protein Revealed with Femtosecond Mid-Infrared Spectroscopy. *Biochemistry 42*, 10054−10059.
(33) Mataga, N., Chosrowjan, H., Taniguchi, S., Hamada, N., Tokunaga, F., Imamoto, Y., and Kataoka, M. (2003) Ultrafast photoreactions in protein nanospaces as revealed by fs fluorescence dynamics measurements on photoactive yellow protein and related systems. *Phys. Chem. Chem. Phys. 5*, 2454−2460.
(34) Chosrowjan, H., Taniguchi, S., Mataga, N., Unno, M., Yamauchi, S., Hamada, N., Kumauchi, M., and Tokunaga, F. (2004) Low-frequency vibrations and their role in ultrafast photoisomerization reaction dynamics of photoactive yellow protein. *J. Phys. Chem. B 108*, 2686−2698.
(35) Larsen, D. S., van Stokkum, I. H. M., Vengris, M., van der Horst, M. A., de Weerd, F. L., Hellingwerf, K. J., and van Grondelle, R. (2004) Incoherent Manipulation of the Photoactive Yellow Protein Photocycle with Dispersed Pump-Dump-Probe Spectroscopy. *Biophys. J. 87*, 1858−1872.
(36) Vengris, M., van der Horst, M. A., Zgrablić, G., van Stokkum, I. H. M., Haacke, S., Chergui, M., Hellingwerf, K. J., van Grondelle, R., and Larsen, D. S. (2004) Contrasting the Excited-State Dynamics of the Photoactive Yellow Protein Chromophore: Protein versus Solvent Environments. *Biophys. J. 87*, 1848−1857.
(37) Borucki, B., Otto, H., Meyer, T. E., Cusanovich, M. A., and Heyn, M. P. (2005) Sensitive circular dichroism marker for the chromophore environment of photoactive yellow protein: Assignment of the 307 and 318 nm bands to the n ->pi* transition of the carbonyl. *J. Phys. Chem. B 109*, 629−633.
(38) Heyne, K., Mohammed, O. F., Usman, A., Dreyer, J., Nibbering, E. T. J., and Cusanovich, M. A. (2005) Structural Evolution of the Chromophore in the Primary Stages of Trans/Cis Isomerization in Photoactive Yellow Protein. *J. Am. Chem. Soc. 127*, 18100−18106.
(39) Ihee, H., Rajagopal, S., Šrajer, V., Pahl, R., Anderson, S., Schmidt, M., Schotte, F., Anfinrud, P. A., Wulff, M., and Moffat, K. (2005) Visualizing reaction pathways in photoactive yellow protein from nanoseconds to seconds. *Proc. Natl. Acad. Sci. U. S. A. 102*, 7145−7150.
(40) Vengris, M., Larsen, D. S., van der Horst, M. A., Larsen, O. F. A., Hellingwerf, K. J., and van Grondelle, R. (2005) Ultrafast dynamics of isolated model photoactive yellow protein chromophores: "Chemical perturbation theory" in the laboratory. *J. Phys. Chem. B 109*, 4197−4208.
(41) Espagne, A., Changenet-Barret, P., Plaza, P., and Martin, M. M. (2006) Solvent effect on the excited-state dynamics of analogues of the photoactive yellow protein chromophore. *J. Phys. Chem. A 110*, 3393−3404.
(42) van Stokkum, I. H., Gobets, B., Gensch, T., Mourik, F., Hellingwerf, K. J., Grondelle, R., and Kennis, J. T. (2006) Sub)-picosecond spectral evolution of fluorescence in photoactive proteins studied with a synchroscan streak camera system. *Photochem. Photobiol. 82*, 380−388.
(43) van Wilderen, L. J. G. W., van der Horst, M. A., van Stokkum, I. H. M., Hellingwerf, K. J., van Grondelle, R., and Groot, M. L. (2006) Ultrafast infrared spectroscopy reveals a key step for successful entry into the photocycle for photoactive yellow protein. *Proc. Natl. Acad. Sci. U. S. A. 103*, 15050−15055.
(44) Nakamura, R., Hamada, N., Ichida, H., Tokunaga, F., and Kanematsu, Y. (2007) Ultrafast dynamics of photoactive yellow protein via the photoexcitation and emission processes. *Photochem. Photobiol. 83*, 397−402.
(45) Nakamura, R., Hamada, N., Ichida, H., Tokunaga, F., and Kanematsu, Y. (2007) Coherent oscillations in ultrafast fluorescence of photoactive yellow protein. *J. Chem. Phys. 127*, 215102.
(46) Coureux, P. D., Fan, Z. P., Stojanoff, V., and Genick, U. K. (2008) Picometer-scale conformational heterogeneity separates functional from nonfunctional states of a photoreceptor protein. *Structure 16*, 863−872.
(47) Nakamura, R., Hamada, N., Ichida, H., Tokunaga, F., and Kanematsu, Y. (2008) Transient vibronic structure in ultrafast fluorescence spectra of photoactive yellow protein. *Photochem. Photobiol. 84*, 937−940.
(48) Carroll, E. C., Hospes, M., Valladares, C., Hellingwerf, K. J., and Larsen, D. S. (2011) Is the photoactive yellow protein a UV-B/blue light photoreceptor? *Photochemical & Photobiological Sciences 10*, 464−468.
(49) Rupenyan, A. B., Vreede, J., van Stokkum, I. H. M., Hospes, M., Kennis, J. T. M., Hellingwerf, K. J., and Groot, M. L. (2011) Proline 68 Enhances Photoisomerization Yield in Photoactive Yellow Protein. *J. Phys. Chem. B 115*, 6668−6677.
(50) Nakamura, R., Hamada, N., Abe, K., and Yoshizawa, M. (2012) Ultrafast Hydrogen-Bonding Dynamics in the Electronic Excited State of Photoactive Yellow Protein Revealed by Femtosecond Stimulated Raman Spectroscopy. *J. Phys. Chem. B 116*, 14768−14775.
(51) Schotte, F., Cho, H. S., Kaila, V. R. I., Kamikubo, H., Dashdorj, N., Henry, E. R., Graber, T. J., Henning, R., Wulff, M., Hummer, G., Kataoka, M., and Anfinrud, P. A. (2012) Watching a signaling protein function in real time via 100-ps time-resolved Laue crystallography. *Proc. Natl. Acad. Sci. U. S. A. 109*, 19256−19261.
(52) Jung, Y. O., Lee, J. H., Kim, J., Schmidt, M., Moffat, K., Šrajer, V., and Ihee, H. (2013) Volume-conserving trans-cis isomerization

DOI: 10.1021/acs.biochem.7b01114
Biochemistry XXXX, XXX, XXX−XXX

pathways in photoactive yellow protein visualized by picosecond X-ray crystallography. *Nat. Chem. 5*, 212−220.
(53) Liu, J., Yabushita, A., Taniguchi, S., Chosrowjan, H., Imamoto, Y., Sueda, K., Miyanaga, N., and Kobayashi, T. (2013) Ultrafast Time-Resolved Pump−Probe Spectroscopy of PYP by a Sub-8 fs Pulse Laser at 400 nm. *J. Phys. Chem. B 117*, 4818−4826.
(54) Naseem, S., Laurent, A. D., Carroll, E. C., Vengris, M., Kumauchi, M., Hoff, W. D., Krylov, A. I., and Larsen, D. S. (2013) Photo-isomerization upshifts the pKa of the Photoactive Yellow Protein chromophore to contribute to photocycle propagation. *J. Photochem. Photobiol., A 270*, 43−52.
(55) Schmidt, M., Srajer, V., Henning, R., Ihee, H., Purwar, N., Tenboer, J., and Tripathi, S. (2013) Protein energy landscapes determined by five-dimensional crystallography. *Acta Crystallogr., Sect. D: Biol. Crystallogr. 69*, 2534−2542.
(56) Zhu, J., Paparelli, L., Hospes, M., Arents, J., Kennis, J. T. M., van Stokkum, I. H. M., Hellingwerf, K. J., and Groot, M. L. (2013) Photoionization and Electron Radical Recombination Dynamics in Photoactive Yellow Protein Investigated by Ultrafast Spectroscopy in the Visible and Near-Infrared Spectral Region. *J. Phys. Chem. B 117*, 11042−11048.
(57) Tenboer, J., Basu, S., Zatsepin, N., Pande, K., Milathianaki, D., Frank, M., Hunter, M., Boutet, S., Williams, G. J., Koglin, J. E., Oberthuer, D., Heymann, M., Kupitz, C., Conrad, C., Coe, J., Roy-Chowdhury, S., Weierstall, U., James, D., Wang, D., Grant, T., Barty, A., Yefanov, O., Scales, J., Gati, C., Seuring, C., Srajer, V., Henning, R., Schwander, P., Fromme, R., Ourmazd, A., Moffat, K., Van Thor, J. J., Spence, J. C. H., Fromme, P., Chapman, H. N., and Schmidt, M. (2014) Time-resolved serial crystallography captures high-resolution intermediates of photoactive yellow protein. *Science 346*, 1242−1246.
(58) Zhu, J., Vreede, J., Hospes, M., Arents, J., Kennis, J. T. M., van Stokkum, I. H. M., Hellingwerf, K. J., and Groot, M. L. (2015) Short Hydrogen Bonds and Negative Charge in Photoactive Yellow Protein Promote Fast Isomerization but not High Quantum Yield. *J. Phys. Chem. B 119*, 2372−2383.
(59) Mix, L. T., Kirpich, J., Kumauchi, M., Ren, J., Vengris, M., Hoff, W. D., and Larsen, D. S. (2016) Bifurcation in the Ultrafast Dynamics of the Photoactive Yellow Proteins from *Leptospira biflexa* and *Halorhodospira halophila*. *Biochemistry 55*, 6138−6149.
(60) Pande, K., Hutchison, C. D. M., Groenhof, G., Aquila, A., Robinson, J. S., Tenboer, J., Basu, S., Boutet, S., DePonte, D. P., Liang, M., White, T. A., Zatsepin, N. A., Yefanov, O., Morozov, D., Oberthuer, D., Gati, C., Subramanian, G., James, D., Zhao, Y., Koralek, J., Brayshaw, J., Kupitz, C., Conrad, C., Roy-Chowdhury, S., Coe, J. D., Metz, M., Xavier, P. L., Grant, T. D., Koglin, J. E., Ketawala, G., Fromme, R., Šrajer, V., Henning, R., Spence, J. C. H., Ourmazd, A., Schwander, P., Weierstall, U., Frank, M., Fromme, P., Barty, A., Chapman, H. N., Moffat, K., van Thor, J. J., and Schmidt, M. (2016) Femtosecond structural dynamics drives the trans/cis isomerization in photoactive yellow protein. *Science 352*, 725−729.
(61) Rajagopal, S., Anderson, S., Srajer, V., Schmidt, M., Pahl, R., and Moffat, K. (2005) A structural pathway for signaling in the E46Q mutant of photoactive yellow protein. *Structure 13*, 55−63.
(62) Devanathan, S., Pacheco, A., Ujj, L., Cusanovich, M., Tollin, G., Lin, S., and Woodbury, N. (1999) Femtosecond spectroscopic observations of initial intermediates in the photocycle of the photoactive yellow protein from Ectothiorhodospira halophila. *Biophys. J. 77*, 1017−1023.
(63) Kim, P. W., Freer, L. H., Rockwell, N. C., Martin, S. S., Lagarias, J. C., and Larsen, D. S. (2012) Femtosecond Photodynamics of the Red/Green Cyanobacteriochrome NpR6012g4 from *Nostoc punctiforme*. 1. Forward Dynamics. *Biochemistry 51*, 608−618.
(64) Heyne, K., Herbst, J., Stehlik, D., Esteban, B., Lamparter, T., Hughes, J., and Diller, R. (2002) Ultrafast Dynamics of Phytochrome from the Cyanobacterium *Synechocystis*, Reconstituted with Phycocyanobilin and Phycoerythrobilin. *Biophys. J. 82*, 1004−1016.
(65) Kim, P. W., Freer, L. H., Rockwell, N. C., Martin, S. S., Lagarias, J. C., and Larsen, D. S. (2012) Femtosecond Photodynamics of the Red/Green Cyanobacteriochrome NpR6012g4 from *Nostoc punctiforme*. 2. Reverse Dynamics. *Biochemistry 51*, 619−630.
(66) Larsen, D. S., Papagiannakis, E., van Stokkum, I. H. M., Vengris, M., Kennis, J. T. M., and van Grondelle, R. (2003) Excited state dynamics of beta-carotene explored with dispersed multi-pulse transient absorption. *Chem. Phys. Lett. 381*, 733−742.
(67) Imamoto, Y., Ito, T., Kataoka, M., and Tokunaga, F. (1995) Reconstitution photoactive yellow protein from apoprotein and p-coumaric acid derivatives. *FEBS Lett. 374*, 157−160.
(68) Mihara, K. i., Hisatomi, O., Imamoto, Y., Kataoka, M., and Tokunaga, F. (1997) Functional Expression and Site-Directed Mutagenesis of Photoactive Yellow Protein. *J. Biochem. 121*, 876−880.
(69) Gottlieb, S. M., Kim, P. W., Rockwell, N. C., Hirose, Y., Ikeuchi, M., Lagarias, J. C., and Larsen, D. S. (2013) Primary Photodynamics of the Green/Red-Absorbing Photoswitching Regulator of the Chromatic Adaptation E Domain from *Fremyella diplosiphon*. *Biochemistry 52*, 8198−8208.
(70) Mix, L. T., Hara, M., Rathod, R., Kumauchi, M., Hoff, W. D., and Larsen, D. S. (2016) Non-Canonical Photocycle Initiation Dynamics of the Photoactive Yellow Protein Domain of the PYP-Phytochrome-Related (Ppr) Photoreceptor. *J. Phys. Chem. Lett. 7*, 5212−5218.
(71) Yamaguchi, S., Kamikubo, H., Kurihara, K., Kuroki, R., Niimura, N., Shimizu, N., Yamazaki, Y., and Kataoka, M. (2009) Low-barrier hydrogen bond in photoactive yellow protein. *Proc. Natl. Acad. Sci. U. S. A. 106*, 440−444.
(72) Berendsen, H. J. C., Postma, J. P. M., van Gunsteren, W. F., DiNola, A., and Haak, J. R. (1984) Molecular dynamics with coupling to an external bath. *J. Chem. Phys. 81*, 3684−3690.
(73) Bussi, G., Donadio, D., and Parrinello, M. (2007) Canonical sampling through velocity rescaling. *J. Chem. Phys. 126*, 014101.
(74) Hess, B., Bekker, H., Berendsen, H. J. C., and Fraaije, J. G. E. M. (1997) LINCS: A linear constraint solver for molecular simulations. *J. Comput. Chem. 18*, 1463−1472.
(75) Miyamoto, S., and Kollman, P. A. (1992) Settle: An analytical version of the SHAKE and RATTLE algorithm for rigid water models. *J. Comput. Chem. 13*, 952−962.
(76) Essmann, U., Perera, L., Berkowitz, M. L., Darden, T., Lee, H., and Pedersen, L. G. (1995) A smooth particle mesh Ewald method. *J. Chem. Phys. 103*, 8577−8593.
(77) van der Spoel, D., Lindahl, E., Hess, B., Groenhof, G., Mark, A. E., and Berendsen, H. J. C. (2005) GROMACS: Fast, flexible, and free. *J. Comput. Chem. 26*, 1701−1718.
(78) Duan, Y., Wu, C., Chowdhury, S., Lee, M. C., Xiong, G., Zhang, W., Yang, R., Cieplak, P., Luo, R., Lee, T., Caldwell, J., Wang, J., and Kollman, P. (2003) A point-charge force field for molecular mechanics simulations of proteins based on condensed-phase quantum mechanical calculations. *J. Comput. Chem. 24*, 1999−2012.
(79) Schmidt, M. W., Baldridge, K. K., Boatz, J. A., Elbert, S. T., Gordon, M. S., Jensen, J. H., Koseki, S., Matsunaga, N., Nguyen, K. A., Su, S., Windus, T. L., Dupuis, M., and Montgomery, J. A. (1993) General atomic and molecular electronic structure system. *J. Comput. Chem. 14*, 1347−1363.
(80) Adamo, C., and Barone, V. (1999) Toward reliable density functional methods without adjustable parameters: The PBE0 model. *J. Chem. Phys. 110*, 6158−6170.
(81) Granovsky, A. A. (2011) Extended multi-configuration quasi-degenerate perturbation theory: The new approach to multi-state multi-reference perturbation theory. *J. Chem. Phys. 134*, 214113.
(82) Roos, B. O., Taylor, P. R., and Siegbahn, P. E. M. (1980) A complete active space SCF method (CASSCF) using a density matrix formulated super-CI approach. *Chem. Phys. 48*, 157−173.
(83) Granovsky, A. A. *Firefly*, version 8.2.0 (http://classic.chem.msu.su/gran/firefly/index.html).
(84) van Stokkum, I. H. M., Larsen, D. S., and van Grondelle, R. (2004) Global and target analysis of time-resolved spectra. *Biochim. Biophys. Acta, Bioenerg. 1657*, 82−104.

DOI: 10.1021/acs.biochem.7b01114
Biochemistry XXXX, XXX, XXX−XXX

(85) Holzwarth, A. (1996) Data Analysis of Time-Resolved Measurements. In *Biophysical Techniques in Photosynthesis* (Amesz, J., and Hoff, A., Eds.) pp 75−92, Springer, Dordrecht, The Netherlands.
(86) Carroll, E. C., Song, S.-H., Kumauchi, M., van Stokkum, I. H. M., Jailaubekov, A., Hoff, W. D., and Larsen, D. S. (2010) Subpicosecond Excited-State Proton Transfer Preceding Isomerization During the Photorecovery of Photoactive Yellow Protein. *J. Phys. Chem. Lett. 1*, 2793−2799.
(87) Changenet-Barret, P., Plaza, P., Martin, M. M., Chosrowjan, H., Taniguchi, S., Mataga, N., Imamoto, Y., and Kataoka, M. (2009) Structural Effects on the Ultrafast Photoisomerization of Photoactive Yellow Protein. Transient Absorption Spectroscopy of Two Point Mutants. *J. Phys. Chem. C 113*, 11605−11613.
(88) Schultz, T., Quenneville, J., Levine, B., Toniolo, A., Martínez, T. J., Lochbrunner, S., Schmitt, M., Shaffer, J. P., Zgierski, M. Z., and Stolow, A. (2003) Mechanism and Dynamics of Azobenzene Photoisomerization. *J. Am. Chem. Soc. 125*, 8098−8099.
(89) Rudolf, P., Kanal, F., Knorr, J., Nagel, C., Niesel, J., Brixner, T., Schatzschneider, U., and Nuernberger, P. (2013) Ultrafast Photochemistry of a Manganese-Tricarbonyl CO-Releasing Molecule (CORM) in Aqueous Solution. *J. Phys. Chem. Lett. 4*, 596−602.
(90) Gromov, E. V., Burghardt, I., Koppel, H., and Cederbaum, L. S. (2007) Electronic structure of the PYP chromophore in its native protein environment. *J. Am. Chem. Soc. 129*, 6798−6806.
(91) Coto, P. B., Marti, S., Oliva, M., Olivucci, M., Merchan, M., and Andres, J. (2008) Origin of the absorption maxima of the photoactive yellow protein resolved via ab initio multiconfigurational methods. *J. Phys. Chem. B 112*, 7153−7156.
(92) Ryan, W. L., Gordon, D. J., and Levy, D. H. (2002) Gas-Phase Photochemistry of the Photoactive Yellow Protein Chromophore trans-p-Coumaric Acid. *J. Am. Chem. Soc. 124*, 6194−6201.
(93) de Groot, M., and Buma, W. J. (2005) Comment on "Gas-Phase Photochemistry of the Photoactive Yellow Protein Chromophore trans-p-Coumaric Acid. *J. Phys. Chem. A 109*, 6135−6136.
(94) Kovalenko, S. A., and Dobryakov, A. L. (2013) On the excitation wavelength dependence and Arrhenius behavior of stilbene isomerization rates in solution. *Chem. Phys. Lett. 570*, 56−60.
(95) Kim, J. E., Tauber, M. J., and Mathies, R. A. (2001) Wavelength Dependent Cis-Trans Isomerization in Vision. *Biochemistry 40*, 13774−13778.
(96) Frauenfelder, H., Chen, G., Berendzen, J., Fenimore, P. W., Jansson, H., McMahon, B. H., Stroe, I. R., Swenson, J., and Young, R. D. (2009) A unified model of protein dynamics. *Proc. Natl. Acad. Sci. U. S. A. 106*, 5129−5134.
(97) Bu, Z., and Callaway, D. J. E. (2011) Chapter 5: Proteins MOVE! Protein dynamics and long-range allostery in cell signaling. In *Advances in Protein Chemistry and Structural Biology* (Rossen, D., Ed.) pp 163−221, Academic Press.
(98) Morozov, D., and Groenhof, G. (2016) Hydrogen Bond Fluctuations Control Photochromism in a Reversibly Photo-Switchable Fluorescent Protein. *Angew. Chem., Int. Ed. 55*, 576−578.
(99) Groenhof, G., Schäfer, L. V., Boggio-Pasqua, M., Grubmüller, H., and Robb, M. A. (2008) Arginine52 Controls the Photoisomerization Process in Photoactive Yellow Protein. *J. Am. Chem. Soc. 130*, 3250−3251.
(100) Ko, C., Virshup, A. M., and Martinez, T. J. (2008) Electrostatic control of photoisomerization in the photoactive yellow protein chromophore: Ab initio multiple spawning dynamics. *Chem. Phys. Lett. 460*, 272−277.
(101) Fisher, S. Z., Anderson, S., Henning, R., Moffat, K., Langan, P., Thiyagarajan, P., and Schultz, A. J. (2007) Neutron and X-ray structural studies of short hydrogen bonds in photoactive yellow protein (PYP). *Acta Crystallogr., Sect. D: Biol. Crystallogr. 63*, 1178−1184.
(102) Yonezawa, K., Shimizu, N., Kurihara, K., Yamazaki, Y., Kamikubo, H., and Kataoka, M. (2017) Neutron crystallography of photoactive yellow protein reveals unusual protonation state of Arg52 in the crystal. *Sci. Rep. 7*, 9361.
(103) Yoshimura, Y., Oktaviani, N. A., Yonezawa, K., Kamikubo, H., and Mulder, F. A. A. (2017) Unambiguous Determination of Protein Arginine Ionization States in Solution by NMR Spectroscopy. *Angew. Chem., Int. Ed. 56*, 239−242.
(104) Graen, T., Inhester, L., Clemens, M., Grubmüller, H., and Groenhof, G. (2016) The Low Barrier Hydrogen Bond in the Photoactive Yellow Protein: A Vacuum Artifact Absent in the Crystal and Solution. *J. Am. Chem. Soc. 138*, 16620−16631.
(105) Changenet-Barret, P., Plaza, P., Martin, M. M., Chosrowjan, H., Taniguchi, S., Mataga, N., Imamoto, Y., and Kataoka, M. (2007) Role of arginine 52 on the primary photoinduced events in the PYP photocycle. *Chem. Phys. Lett. 434*, 320−325.
(106) Chosrowjan, H., Mataga, N., Shibata, Y., Imamoto, Y., and Tokunaga, F. (1998) Environmental effects on the femtosecond-picosecond fluorescence dynamics of photoactive yellow protein: Chromophores in aqueous solutions and in protein nanospaces modified by site-directed mutagenesis. *J. Phys. Chem. B 102*, 7695−7698.
(107) Mataga, N., Chosrowjan, H., Shibata, Y., Imamoto, Y., and Tokunaga, F. (2000) Effects of modification of protein nanospace structure and change of temperature on the femtosecond to picosecond fluorescence dynamics of photoactive yellow protein. *J. Phys. Chem. B 104*, 5191−5199.
(108) Takeshita, K., Imamoto, Y., Kataoka, M., Mihara, K., Tokunaga, F., and Terazima, M. (2002) Structural change of site-directed mutants of PYP: New dynamics during pR state. *Biophys. J. 83*, 1567−1577.
(109) Düx, P., Rubinstenn, G., Vuister, G. W., Boelens, R., Mulder, F. A. A., Hård, K., Hoff, W. D., Kroon, A. R., Crielaard, W., Hellingwerf, K. J., and Kaptein, R. (1998) Solution Structure and Backbone Dynamics of the Photoactive Yellow Protein. *Biochemistry 37*, 12689−12699.
(110) Groenhof, G., Lensink, M. F., Berendsen, H. J. C., Snijders, J. G., and Mark, A. E. (2002) Signal transduction in the photoactive yellow protein. I. Photon absorption and the isomerization of the chromophore. *Proteins: Struct., Funct., Genet. 48*, 202−211.
(111) Groenhof, G., Bouxin-Cademartory, M., Hess, B., de Visser, S. P., Berendsen, H. J. C., Olivucci, M., Mark, A. E., and Robb, M. A. (2004) Photoactivation of the Photoactive Yellow Protein: Why Photon Absorption Triggers a Trans-to-Cis Isomerization of the Chromophore in the Protein. *J. Am. Chem. Soc. 126*, 4228−4233.
(112) Bernard, C., Houben, K., Derix, N. M., Marks, D., van der Horst, M. A., Hellingwerf, K. J., Boelens, R., Kaptein, R., and van Nuland, N. A. J. (2005) The Solution Structure of a Transient Photoreceptor Intermediate: Δ25 Photoactive Yellow Protein. *Structure 13*, 953−962.
(113) Taenzler, P. J., Sadeghian, K., and Ochsenfeld, C. (2016) A Dynamic Equilibrium of Three Hydrogen-Bond Conformers Explains the NMR Spectrum of the Active Site of Photoactive Yellow Protein. *J. Chem. Theory Comput. 12*, 5170−5178.
(114) Hutchison, C. D. M., and van Thor, J. J. (2017) Populations and coherence in femtosecond time resolved X-ray crystallography of the photoactive yellow protein. *Int. Rev. Phys. Chem. 36*, 117−143.
(115) Changenet-Barret, P., Plaza, P., Martin, M. M., Chosrowjan, H., Taniguchi, S., Mataga, N., Imamoto, Y., and Kataoka, M. (2007) Role of arginine 52 on the primary photoinduced events in the PYP photocycle. *Chem. Phys. Lett. 434*, 320−325.
(116) Kasha, M. (1950) Characterization of electronic transitions in complex molecules. *Discuss. Faraday Soc. 9*, 14−19.

DOI: 10.1021/acs.biochem.7b01114
Biochemistry XXXX, XXX, XXX−XXX